

# Interseries transitions between Rydberg excitons in Cu<sub>2</sub>O

Sjard Ole Krüger<sup>1,\*</sup> and Stefan Scheel<sup>1</sup>

<sup>1</sup>*Institut für Physik, Universität Rostock, Albert-Einstein-Straße 23-24, D-18059 Rostock, Germany*

(Dated: August 5, 2019)

We investigate the infrared optical transitions between excitons of the yellow, green and blue series in the cuprous oxide Cu<sub>2</sub>O. We show that, in many cases, the dipole approximation is inadequate and, in particular, that it breaks down in yellow-blue transitions even for moderate principal quantum numbers of  $n \approx 10$ . The interband matrix elements of the transition operator needed for the evaluation of the excitonic transition strengths are derived from known as well as from fitted band parameters.

PACS numbers: 78.20.Bh, 71.35.-y, 71.20.-Nr

## I. INTRODUCTION

Excitons, bound states of electrons and holes in semiconductors, have first been postulated by Frenkel<sup>1</sup> in the limit of strongly bound systems, and Wannier<sup>2</sup> in the weakly bound limit. For the Wannier excitons, the crystal mostly acts as a dielectric background, and the excitonic states show remarkable similarities to those of the hydrogen atom. The first observation of the Wannier excitons succeeded in the yellow series of Cu<sub>2</sub>O in the 1950s<sup>3</sup> reaching up to principal quantum numbers of  $n = 8$ . Recently, this limit has been pushed up to  $n = 25$ <sup>4</sup> and orbital quantum numbers of  $\ell = 5$ <sup>5</sup>, revealing an almost perfect Rydberg series. The nonparabolicity of the valence band does, however, induce a systematic deviation from the Rydberg series, which can be cast into quantum defects  $\delta_{n,\ell}$ <sup>6,7</sup> approaching constant values for large  $n$  similar to alkali Rydberg atoms.

Since the first observation of these excitonic Rydberg states, they have attracted considerable attention due to their exaggerated properties such as their large real-space extensions, comparatively long lifetimes and huge polarisabilities. The latter is responsible for the Rydberg blockade phenomenon already observed early on<sup>4</sup> due to the dipole-dipole interaction of the yellow Rydberg excitons<sup>8</sup>, but it also contributes to a strong interaction with the electron-hole plasma<sup>9</sup>. Further investigations have focussed on the influence of the valence-band structure on the excitonic quantum defects<sup>7,10</sup>, the interaction with phonons and photons<sup>11</sup>, the influence of electric and magnetic fields<sup>6,12</sup> as well as the possibility to observe giant-dipole excitons in crossed electromagnetic fields<sup>13</sup>. Moreover, the level statistics<sup>14,15</sup> has been investigated showing the breaking of all anti-unitary symmetries.

In addition to the yellow exciton series, there are three more excitonic series in Cu<sub>2</sub>O (see Fig. 1) that have been found as early as the 1950s and 1960s<sup>16,17</sup>. Transitions between the ground states of the yellow and blue series have been observed as polaritonic beating<sup>18</sup>, and intraseries transitions within the yellow series have been probed<sup>19</sup>. More recently, proposals have been put forward to use the yellow intraseries transitions for the implementation of tunable excitonic masers<sup>20,21</sup>. Further-

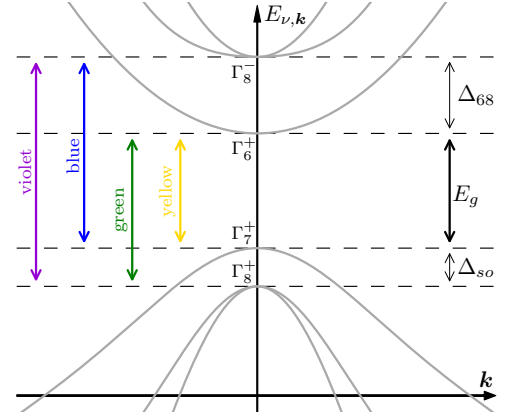


FIG. 1: Schematic band structure of Cu<sub>2</sub>O in the vicinity of the  $\Gamma$ -point and the main band gap.

more, the photoluminescence of the excitons in Cu<sub>2</sub>O has been measured, including both the blue and violet series<sup>22</sup> and the superradiance-to-polariton crossover of the blue  $1S$  state has been investigated in dependence of the crystal thickness<sup>23</sup>. As the Rydberg excitons show coherent features already in single-photon absorption<sup>24</sup>, the pertinent question is how to exploit these in coherent manipulation schemes such as EIT-based protocols for single-photon generation<sup>25</sup> or to generate giant optical nonlinearities<sup>26</sup>. The first step in this direction is to identify suitable dipole-allowed transitions that are also easily accessible experimentally. As the excitonic Rydberg energies of Cu<sub>2</sub>O are very low compared to atomic systems, intraseries transitions are inconveniently located in the far infrared. However, transitions between different exciton series, i.e. interseries transitions, could be exploited. In particular, transitions between Rydberg states of different exciton series become accessible with near-infrared light.

In this article, we compute the infrared transition strengths from the yellow  $P$ -excitons into the green and blue excitons as shown in Fig. 2. These transition strengths are directly proportional to both the transi-

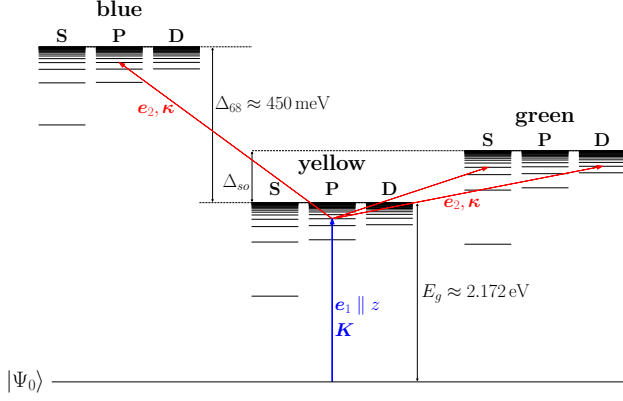


FIG. 2: Schematic term diagram of the excitonic states in the yellow, green and blue series of  $\text{Cu}_2\text{O}$ . In the proposed scheme, the  $z$ -component of a yellow  $\Gamma_4^-$   $P$ -exciton is excited via a  $z$ -polarised laser beam with wave vector  $\mathbf{K}$ , and the transitions into the green and blue series are probed by a second laser beam with polarisation  $\mathbf{e}_2$  and wave vector  $\mathbf{\kappa}$ .  $|\Psi_0\rangle$  denotes the crystal vacuum.

TABLE I: Material properties of  $\text{Cu}_2\text{O}$  used in this work.

$B_{6,8}$	$0.342 \hbar\pi a_g^{-1}$		$A_1$	$-1.76$	
$A_6$	2.44	this work	$A_2$	4.519	
$A_8$	3.99		$A_3$	$-2.201$	$_6$
$E_g$	2.17208 eV	$^4$	$B_1$	0.02	
$\Delta_{68}$	450 meV	$^{18}$	$B_2$	$-0.022$	
$\Delta_{so}$	131 meV	$^3$	$B_3$	$-0.202$	
$a_g$	0.427 nm	$^{27}$	$\varepsilon_s$	7.5	$^{28}$
$F$	$-0.43$	$^{12}$ (see App. A)	$\varepsilon_\infty$	6.46	$^{29}$

tion rate per exciton and the line intensities of the corresponding transitions. For transitions between Rydberg states of different series, the dipole approximation breaks down as the states can reach real-space extensions up to  $\mu\text{m}$  while the separation in energy approaches a finite value ( $\Delta_{so} = 131 \text{ meV}$  from yellow to green and  $\Delta_{68} \approx 450 \text{ meV}$  from yellow to blue, see also Tab. I). Therefore, the spatial extent of the excitons becomes comparable to the wavelength, in which case the dipole approximation is known to break down. We will first calculate the transition strengths in dipole approximation and subsequently assess the influence of the breakdown of the dipole approximation for a representative set of transitions.

This article is structured as follows. In Sec. II the general theory of excitonic interseries transitions is laid out both with and without the dipole approximation. Section III contains the derivation of the inter-band matrix elements of the light-matter coupling operator that are needed for the evaluation of the transition strengths. Sections IV and V contain the derivation and discussion

TABLE II: Estimates of the properties of the excitonic series, derived from the values in Tab. I and Eq. (17). The experimental Rydberg energies of the green and blue series are based on only a few low- $n$  states and thus not very reliable.

	$m_h$	$m_e$	$a_B/\text{nm}$	$Ry^*/\text{meV}$	$Ry_{\text{exp}}^*/\text{meV}$
yellow	$\frac{-m_0}{A_1-2B_1}$	$\frac{m_0}{A_6 - \frac{4B_{6,8}^2}{3m_0\Delta_{68}}}$	1.12	86.07	$86.04^7$
green	$\frac{-m_0}{A_1+B_1}$	$\frac{m_0}{A_6 - \frac{4B_{6,8}^2}{3m_0\Delta_{68}}}$	1.09	87.94	$139^{30}$
blue	$\frac{-m_0}{A_1-2B_1}$	$\frac{m_0}{A_8 + \frac{2B_{6,8}^2}{3m_0\Delta_{68}}}$	2.58	37.22	$46^{17}$

of the transition strengths from the yellow series to the green and blue series, respectively, followed by an outlook on future work as well as a discussion of the results in Sec. VI. Computational details such as the chosen basis states and the conduction-band Hamiltonian have been delegated to the Appendix.

## II. EXCITON STATES AND TRANSITION OPERATORS

In this section, the general structure of the transition matrix-elements of excitonic interseries transitions will be derived. The excitons are comprised of a bound pair of an electron in the conduction band and a hole in the valence band. Their quantum states can be written as

$$|\Psi_{\tau,\mathbf{K}}^{c,v}\rangle = \sum_{\mathbf{k}} \phi_{\tau,\mathbf{K}}(\mathbf{k}) \hat{a}_{c,\mathbf{k}+\alpha\mathbf{K}}^\dagger \hat{a}_{v,\mathbf{k}-\beta\mathbf{K}} |\Psi_0\rangle. \quad (1)$$

Here,  $\tau = \{n, \ell, m, c, v\}$  labels the quantum numbers of the internal excitonic state with the envelope function  $\phi_{\tau,\mathbf{K}}(\mathbf{k})$ ,  $c$  and  $v$  denote the conduction and valence band with fermionic creation (annihilation) operators  $\hat{a}_{c,\mathbf{q}}^\dagger$  ( $\hat{a}_{v,\mathbf{q}}$ ), and  $|\Psi_0\rangle$  is the crystal vacuum state.  $\mathbf{k}$  and  $\mathbf{K}$  denote the relative and center-of-mass (COM) momenta of the electron and hole with the relative masses  $\alpha = m_e/M$ ,  $\beta = m_h/M$  and  $M = m_e + m_h$ . Mass estimates based on the band parameters are listed in Tab. II.

Note that Eq. (1) is expressed in terms of valence-band electrons, and the actual hole momentum is  $-\mathbf{k} + \beta\mathbf{K}$ . Here and in the following we will always assume that for the COM momenta of interest  $\phi_{\tau,\mathbf{K}}(\mathbf{k}) \approx \phi_{\tau,0}(\mathbf{k}) = \phi_{\tau}(\mathbf{k})$  holds. It should also be noted here that, in general, the excitonic states in Eq. (1) are mixed due to the broken rotational symmetry of the crystal. A better approximation to the actual excitonic states would be the use of properly symmetrised basis states as done in Ref.<sup>31</sup> and discussed in Appendix B. We will continue first the analysis in terms of the basis states in Eq. (1) as the symmetrised states are linear combinations of them, and later use the symmetrised states from Sec. IV onwards.

The full one-electron crystal Hamiltonian is given by

$$H = \frac{\mathbf{p}^2}{2m_0} + V(r) + \frac{\hbar}{4m_0^2 c^2} (\mathbf{S} \times \nabla V) \cdot \mathbf{p} \quad (2)$$

where  $V(r)$  is the crystal-periodic potential containing both the effective interaction with the crystal ions and the other electrons, and  $\mathbf{S}$  denotes the Pauli matrices. The minimal substitution yields a light-matter coupling operator of the form

$$\frac{e\mathbf{A}(\mathbf{r})}{m_0} \cdot \left( \mathbf{p} + \frac{\hbar}{4m_0 c^2} (\mathbf{S} \times \nabla V) \right) = \frac{e\mathbf{A}(\mathbf{r})}{m_0} \cdot \boldsymbol{\pi} \quad (3)$$

where the Coulomb gauge has been used and the diamagnetic term has been ignored. Even if the components of  $\mathbf{A}(\mathbf{r})$  do not correspond to plane waves, they can be decomposed into them by a Fourier transformation. We will therefore assume the transition operator to be of the form  $e^{-i\boldsymbol{\kappa}\mathbf{r}} \boldsymbol{\pi}$ , which can be expressed in second quantisation as

$$e^{-i\boldsymbol{\kappa}\mathbf{r}} \boldsymbol{\pi} = \sum_{\nu, \nu'} \sum_{\mathbf{k}} \langle \nu, \mathbf{k} | e^{-i\boldsymbol{\kappa}\mathbf{r}} \boldsymbol{\pi} | \nu', \mathbf{k} + \boldsymbol{\kappa} \rangle \hat{a}_{\nu, \mathbf{k}}^\dagger \hat{a}_{\nu', \mathbf{k} + \boldsymbol{\kappa}}, \quad (4)$$

where  $\nu$  and  $\nu'$  sum over the bands of interest and the pseudo-momentum conservation has been used. Umklapp processes are being ignored due to the small magnitude of the wave vectors of interest.

The matrix element  $\langle \Psi_{\tau, \mathbf{K}}^{c, v} | e^{-i\boldsymbol{\kappa}\mathbf{r}} \boldsymbol{\pi} | \Psi_{\tau', \mathbf{K}'}^{c, v'} \rangle$  with  $v \neq v'$  can be evaluated as

$$\begin{aligned} & \langle \Psi_{\tau, \mathbf{K}}^{c, v} | e^{-i\boldsymbol{\kappa}\mathbf{r}} \boldsymbol{\pi} | \Psi_{\tau', \mathbf{K}'}^{c, v'} \rangle \\ &= \sum_{\nu, \nu'} \sum_{\mathbf{q}} \langle \nu, \mathbf{q} | e^{-i\boldsymbol{\kappa}\mathbf{r}} \boldsymbol{\pi} | \nu', \mathbf{q} + \boldsymbol{\kappa} \rangle \sum_{\mathbf{k}, \mathbf{k}'} \phi_{\tau'}(\mathbf{k}') \phi_{\tau}^\dagger(\mathbf{k}) \\ & \quad \times \langle \Psi_0 | \hat{a}_{\nu, \mathbf{k} - \beta\mathbf{K}}^\dagger \hat{a}_{c, \mathbf{k} + \alpha\mathbf{K}} \hat{a}_{\nu, \mathbf{q}}^\dagger \\ & \quad \times \hat{a}_{\nu', \mathbf{q} + \boldsymbol{\kappa}} \hat{a}_{c, \mathbf{k}' + \alpha'\mathbf{K}'}^\dagger \hat{a}_{\nu', \mathbf{k}' - \beta'\mathbf{K}'} | \Psi_0 \rangle. \end{aligned}$$

This corresponds to a change of valence band by the hole, i.e. a transition from the yellow to the green series (see Fig. 1). Using the fact that  $v \neq v'$  implies that only those terms contribute in which  $\nu = v'$  and  $\nu' = v$ , and applying the anti-commutator rules  $[\hat{a}_{\nu, \mathbf{q}}^\dagger, \hat{a}_{\nu', \mathbf{q}'}]_+ = \delta_{\nu, \nu'} \delta_{\mathbf{q}, \mathbf{q}'}$  as well as  $[\hat{a}_{\nu, \mathbf{q}}, \hat{a}_{\nu', \mathbf{q}'}]_+ = [\hat{a}_{\nu, \mathbf{q}}^\dagger, \hat{a}_{\nu', \mathbf{q}'}^\dagger]_+ = 0$  gives

$$\begin{aligned} & \langle \Psi_{\tau, \mathbf{K}}^{c, v} | e^{-i\boldsymbol{\kappa}\mathbf{r}} \boldsymbol{\pi} | \Psi_{\tau', \mathbf{K}'}^{c, v'} \rangle \\ &= - \sum_{\mathbf{q}} \langle v', \mathbf{q} | e^{-i\boldsymbol{\kappa}\mathbf{r}} \boldsymbol{\pi} | v, \mathbf{q} + \boldsymbol{\kappa} \rangle \sum_{\mathbf{k}, \mathbf{k}'} \phi_{\tau'}(\mathbf{k}') \phi_{\tau}^\dagger(\mathbf{k}) \\ & \quad \times \langle \Psi_0 | \hat{a}_{v, \mathbf{k} - \beta\mathbf{K}}^\dagger \hat{a}_{v, \mathbf{q} + \boldsymbol{\kappa}} \hat{a}_{v', \mathbf{q}}^\dagger \hat{a}_{v', \mathbf{k}' - \beta'\mathbf{K}'} \\ & \quad \times \left( \delta_{\mathbf{k}' + \alpha'\mathbf{K}', \mathbf{k} + \alpha\mathbf{K}} - \hat{a}_{c, \mathbf{k}' + \alpha'\mathbf{K}'}^\dagger \hat{a}_{c, \mathbf{k} + \alpha\mathbf{K}} \right) | \Psi_0 \rangle. \quad (5) \end{aligned}$$

The matrix element of the vacuum state in Eq. (5) can only be nonzero if the electrons are created in the same states from which they had been annihilated. In this case, the products of creation and annihilation operator

can be rewritten as the number operator  $\hat{a}_{\nu, \mathbf{q}}^\dagger \hat{a}_{\nu, \mathbf{q}} = \hat{n}_{\nu, \mathbf{q}}$ . The matrix element can then be evaluated by observing that, in the crystal vacuum state, all valence bands are completely filled while the conduction bands are empty,

$$\begin{aligned} & \langle \Psi_{\tau, \mathbf{K}}^{c, v} | e^{-i\boldsymbol{\kappa}\mathbf{r}} \boldsymbol{\pi} | \Psi_{\tau', \mathbf{K}'}^{c, v'} \rangle \\ &= -\delta_{\mathbf{K}' - \boldsymbol{\kappa}, \mathbf{K}} \sum_{\mathbf{k}} \phi_{\tau}^\dagger(\mathbf{k} + \beta\mathbf{K}' + \alpha\boldsymbol{\kappa}) \phi_{\tau'}(\mathbf{k} + \beta'\mathbf{K}') \\ & \quad \times \langle v', \mathbf{k} | e^{-i\boldsymbol{\kappa}\mathbf{r}} \boldsymbol{\pi} | v, \mathbf{k} + \boldsymbol{\kappa} \rangle. \quad (6) \end{aligned}$$

It will be more convenient for the subsequent analysis to reformulate this equation in terms of valence-band holes instead of electrons which implies exchanging  $\langle v', \mathbf{k} | e^{-i\boldsymbol{\kappa}\mathbf{r}} \boldsymbol{\pi} | v, \mathbf{k} + \boldsymbol{\kappa} \rangle$  for  $\langle v, -\mathbf{k} - \boldsymbol{\kappa} | e^{-i\boldsymbol{\kappa}\mathbf{r}} \boldsymbol{\pi} | v', -\mathbf{k} \rangle$  and therefore

$$\begin{aligned} & \langle \Psi_{\tau, \mathbf{K}}^{c, v} | e^{-i\boldsymbol{\kappa}\mathbf{r}} \boldsymbol{\pi} | \Psi_{\tau', \mathbf{K}'}^{c, v'} \rangle \\ &= -\delta_{\mathbf{K}' - \boldsymbol{\kappa}, \mathbf{K}} \sum_{\mathbf{k}} \phi_{\tau}^\dagger(\mathbf{k} + \beta\mathbf{K}' + \alpha\boldsymbol{\kappa}) \phi_{\tau'}(\mathbf{k} + \beta'\mathbf{K}') \\ & \quad \times \langle v, -\mathbf{k} - \boldsymbol{\kappa} | e^{-i\boldsymbol{\kappa}\mathbf{r}} \boldsymbol{\pi} | v', -\mathbf{k} \rangle. \quad (7) \end{aligned}$$

The equivalent matrix element for a change of the conduction band (i.e. from the yellow to the blue series) is

$$\begin{aligned} & \langle \Psi_{\tau, \mathbf{K}}^{c, v} | e^{-i\boldsymbol{\kappa}\mathbf{r}} \boldsymbol{\pi} | \Psi_{\tau', \mathbf{K}'}^{c, v'} \rangle \\ &= \delta_{\mathbf{K}, \mathbf{K}' - \boldsymbol{\kappa}} \sum_{\mathbf{k}} \phi_{\tau}^\dagger(\mathbf{k} - \alpha\mathbf{K}) \phi_{\tau'}(\mathbf{k} - \alpha'\mathbf{K} + \beta'\boldsymbol{\kappa}) \\ & \quad \times \langle c, \mathbf{k} | e^{-i\boldsymbol{\kappa}\mathbf{r}} \boldsymbol{\pi} | c', \mathbf{k} + \boldsymbol{\kappa} \rangle. \quad (8) \end{aligned}$$

Single-photon transitions with a change of both valence and conduction bands (say, from the yellow to the violet series) are forbidden to all orders, as these are two-particle transitions which require at least two photons. In the dipole approximation (ignoring the COM momenta of both excitonic states and the photon  $\mathbf{K} = \mathbf{K}' = \boldsymbol{\kappa} = \mathbf{0}$ ), Eq. (7) reduces to

$$\langle \Psi_{\tau}^{c, v} | \boldsymbol{\pi} | \Psi_{\tau'}^{c, v'} \rangle = - \sum_{\mathbf{k}} \phi_{\tau}^\dagger(\mathbf{k}) \phi_{\tau'}(\mathbf{k}) \langle v, -\mathbf{k} | \boldsymbol{\pi} | v', -\mathbf{k} \rangle. \quad (9)$$

The difference between Eqs. (7) and (9) consists of two effects:

- the non-vertical (i.e. non-dipolar) transitions between the pure Bloch states and
- the relative displacement of the envelope functions by  $(\beta - \beta')\mathbf{K}' + \alpha\boldsymbol{\kappa}$  which corresponds to a non-dipolar transition between the envelope functions.

For states with allowed dipole transitions, the first correction is expected to be only weak, while the second one will significantly lower the transition strengths for states with large principal quantum numbers  $n$ . For transitions between Rydberg states of different series, both  $|\mathbf{K}|$  and

TABLE III: Estimates of the momentum-space displacements for the yellow-green and yellow-blue transitions as well as co-propagating and counter-propagating pump and probe beams.

	co-propagating	counter-propagating
yellow	$(\beta - \beta') \mathbf{K}'  + \alpha \boldsymbol{\kappa} $	$(\beta - \beta') \mathbf{K}'  - \alpha \boldsymbol{\kappa} $
-green	$\approx 0.12 \times 10^{-3} \pi/a_g$	$\approx -0.18 \times 10^{-3} \pi/a_g$
yellow	$(\alpha' - \alpha) \mathbf{K}  - \beta' \boldsymbol{\kappa} $	$(\alpha' - \alpha) \mathbf{K}  + \beta' \boldsymbol{\kappa} $
-blue	$\approx -1.96 \times 10^{-3} \pi/a_g$	$\approx -0.82 \times 10^{-3} \pi/a_g$

$|\boldsymbol{\kappa}|$  become constant while the momentum-space extension decreases  $\propto n^{-1}$ . This implies that the overlap of the envelope functions will vanish and the mentioned approximation is only valid as long as the momentum-space extension of at least one of the excitonic states is much larger than  $(\beta - \beta')\mathbf{K}' + \alpha\boldsymbol{\kappa}$ . Or, to phrase it differently, the real-space extension of at least one of the states has to be much smaller than the transition wavelength in order for the dipole approximation to be valid.

The momentum-space displacements for the yellow-green and yellow-blue transitions are given in Tab. III. The smaller values for the yellow-green transitions result partially from the fact that our estimate for the hole mass of the  $\Gamma_8^+$  valence band is very close to that of the  $\Gamma_7^+$  valence band giving  $\beta - \beta' \approx -0.0078$  and, additionally, from the larger  $\boldsymbol{\kappa}$  of the yellow-blue transitions. This implies that the effects from the breakdown of the dipole approximation will be more prominent for the yellow-blue transitions. The wave numbers are given by  $|\mathbf{k}(E)| = E\sqrt{\varepsilon_\infty}/(\hbar c)$  with the refractive index  $\sqrt{\varepsilon_\infty}$  of  $\text{Cu}_2\text{O}$ . The energy separations were approximated by the band gaps, i.e. by  $E_g$  for  $|\mathbf{K}|$  as well as  $\Delta_{so}$  and  $\Delta_{68}$  for the yellow-green and yellow-blue photon momenta  $|\boldsymbol{\kappa}|$ , respectively.

### III. INTERBAND MATRIX ELEMENTS

In order to proceed with the evaluation of Eqs. (7–9), the interband matrix elements  $\langle \nu, \mathbf{q} | e^{-i(\mathbf{q}' - \mathbf{q})\mathbf{r}} \boldsymbol{\pi} | \nu', \mathbf{q}' \rangle$  as well as the envelope functions  $\phi_\tau(\mathbf{q})$  are required. In this section, the calculation of the matrix elements will be laid out, while the envelope functions will be approximated by properly symmetrised hydrogenic functions with the parameters given in Tab. II.

For the transitions between the yellow and green series in  $\text{Cu}_2\text{O}$ , the relevant valence bands are the uppermost  $\Gamma_7^+$  band and the  $\Gamma_8^+$  band, that both stem from the same  $\Gamma_5^+$  band when the spin is ignored. The interband matrix elements can be rewritten in terms of the lattice periodic

functions  $|u_v, \mathbf{q}\rangle$  via  $|v, \mathbf{q}\rangle = e^{i\mathbf{q}\mathbf{r}} |u_v, \mathbf{q}\rangle$  as

$$\begin{aligned} & \langle \Gamma_7^+, \sigma, -\mathbf{q} - \boldsymbol{\kappa} | e^{-i\boldsymbol{\kappa}\mathbf{r}} \boldsymbol{\pi} | \Gamma_8^+, \sigma', -\mathbf{q} \rangle \\ &= \langle u_{\Gamma_7^+}, \sigma, -\mathbf{q} - \boldsymbol{\kappa} | \boldsymbol{\pi} | u_{\Gamma_8^+}, \sigma', -\mathbf{q} \rangle \\ & - \hbar \mathbf{q} \langle u_{\Gamma_7^+}, \sigma, -\mathbf{q} - \boldsymbol{\kappa} | u_{\Gamma_8^+}, \sigma', -\mathbf{q} \rangle, \end{aligned} \quad (10)$$

where  $\sigma$  and  $\sigma'$  denote the substates of the irreducible representations (“spin”). This can be evaluated in perturbation theory using

$$|u_v, \mathbf{q}\rangle \approx |u_v, 0\rangle + \frac{\hbar}{m_0} \sum_n \frac{|u_n, 0\rangle \langle u_n, 0 | \mathbf{q} \cdot \boldsymbol{\pi} | u_v, 0 \rangle}{E_v(0) - E_n(0)}. \quad (11)$$

The term  $\propto \hbar \mathbf{q}$  in Eq. (10) vanishes for  $\boldsymbol{\kappa} = \mathbf{0}$ , and its lowest-order term is proportional to  $q^2 \boldsymbol{\kappa}$ . As both the  $q$  and  $\boldsymbol{\kappa}$  of interest are small compared to the size of the Brillouin zone, this term will be ignored. The remaining term in Eq. (10) gives

$$\begin{aligned} & \langle u_{\Gamma_7^+}, \sigma, -\mathbf{q} - \boldsymbol{\kappa} | \boldsymbol{\pi} | u_{\Gamma_8^+}, \sigma', -\mathbf{q} \rangle \\ &= \frac{\hbar}{m_0} \sum_n \frac{\langle u_{\Gamma_7^+}, \sigma, 0 | -(\mathbf{q} + \boldsymbol{\kappa}) \cdot \boldsymbol{\pi} | u_n, 0 \rangle \langle u_n, 0 | \boldsymbol{\pi} | u_{\Gamma_8^+}, \sigma', 0 \rangle}{E_{\Gamma_7^+}(0) - E_n(0)} \\ & + \frac{\hbar}{m_0} \sum_n \frac{\langle u_{\Gamma_7^+}, \sigma, 0 | \boldsymbol{\pi} | u_n, 0 \rangle \langle u_n, 0 | -\mathbf{q} \cdot \boldsymbol{\pi} | u_{\Gamma_8^+}, \sigma', 0 \rangle}{E_{\Gamma_8^+}(0) - E_n(0)} \\ & = -\langle u_{\Gamma_7^+}, \sigma, \mathbf{q} | \boldsymbol{\pi} | u_{\Gamma_8^+}, \sigma', \mathbf{q} \rangle \\ & - \frac{\hbar}{m_0} \sum_n \frac{\langle u_{\Gamma_7^+}, \sigma, 0 | \boldsymbol{\kappa} \cdot \boldsymbol{\pi} | u_n, 0 \rangle \langle u_n, 0 | \boldsymbol{\pi} | u_{\Gamma_8^+}, \sigma', 0 \rangle}{E_{\Gamma_7^+}(0) - E_n(0)}. \end{aligned} \quad (12)$$

The term proportional to  $\boldsymbol{\kappa}$  corresponds to higher-order transitions between the Bloch states and can induce quadrupole transitions between excitonic states, while the first term is responsible for the dipole transitions.

Assuming that

$$E_{\Gamma_7^+}(0) - E_n(0) \approx E_{\Gamma_8^+}(0) - E_n(0) \quad (13)$$

for all intermediate states  $|u_n, 0\rangle$ , Eq. (12) can be rewritten as

$$\begin{aligned} & \langle u_{\Gamma_7^+}, \sigma, -\mathbf{q} - \boldsymbol{\kappa} | \boldsymbol{\pi} | u_{\Gamma_8^+}, \sigma', -\mathbf{q} \rangle \\ &= -\frac{m_0}{\hbar} \nabla_{\mathbf{q} + \frac{\boldsymbol{\kappa}}{2}} \left[ \mathcal{H} \left( \mathbf{q} + \frac{\boldsymbol{\kappa}}{2} \right) \right]_{\sigma, \sigma'} - F \hbar \tilde{\mathbf{N}}_{\sigma, \sigma'} \cdot \boldsymbol{\kappa}. \end{aligned} \quad (14)$$

Here,  $F \approx -0.43$  denotes a magnetic band parameter, and the matrices  $\tilde{\mathbf{N}}_{\sigma, \sigma'} \in \mathbb{C}^{3 \times 3}$  can be derived from group-theoretical considerations (see Appendix A). In addition,  $\mathcal{H}(\mathbf{q})$  denotes the Suzuki-Hensel Hamiltonian<sup>32</sup>

$$\begin{aligned} \mathcal{H}(\mathbf{q}) &= -\frac{\Delta_{so}}{3} \mathbf{I} \cdot \mathbf{S} + \frac{\hbar^2}{2m_0} \left\{ [A_1 + B_1 \mathbf{I} \cdot \mathbf{S}] q^2 \right. \\ & + \left[ A_2 \left( I_x^2 - \frac{1}{3} \mathbf{I}^2 \right) + B_2 \left( I_x \sigma_x - \frac{1}{3} \mathbf{I} \cdot \mathbf{S} \right) \right] q_x^2 + \text{c.p.} \\ & \left. + [A_3 (I_x I_y + I_y I_x) + B_3 (I_x \sigma_y + I_y \sigma_x)] \{q_x, q_y\} + \text{c.p.} \right\}, \end{aligned} \quad (15)$$

where  $\mathbf{I}$  is the vector of the spin-1 angular-momentum matrices,  $\mathbf{S}$  the vector of the Pauli matrices and  $\{q_x, q_y\} = (q_x q_y + q_y q_x)/2$  the symmetric product. Furthermore, c.p. stands for cyclic permutation,  $\Delta_{so}$  is the spin-orbit splitting of the valence band, and the  $A_i$  and  $B_i$  are band-structure parameters whose values can be found in Tab. I.

The approximation in Eq. (13) is justified as the intermediate states can only have  $\Gamma_7^-$  or  $\Gamma_8^-$  symmetry, and the next band of such symmetry is removed by about  $20 \Delta_{so}$  from the valence bands. A more in-depth discussion of Eq. (14) as well as the matrices  $\tilde{\mathbf{N}}_{\sigma, \sigma'}$  can be found in Appendix A.

In this manner, the interband matrix elements are easily accessible, once the band structure parameters are known. For the valence bands of  $\text{Cu}_2\text{O}$ , good fits to the Suzuki-Hensel Hamiltonian are available<sup>6</sup>. However, one has to keep in mind that the representation of the Hamiltonian in terms of  $\mathbf{I}$  and  $\mathbf{S}$  implies a basis  $\Gamma_4^- \otimes \Gamma_6^+ = \Gamma_6^- \oplus \Gamma_8^-$ . The valence band states in  $\text{Cu}_2\text{O}$ , however, have the symmetry  $\Gamma_5^+ \otimes \Gamma_6^+ = (\Gamma_2^- \otimes \Gamma_4^-) \otimes \Gamma_6^+ = \Gamma_7^+ \oplus \Gamma_8^+$ . Therefore, one has to be careful when assigning the band states to the rows and columns of the Hamiltonian, and one cannot simply assign them by their eigenvalues of the operators  $\mathbf{J}^2$  and  $J_z$  (where  $\mathbf{J} = \mathbf{I} + \mathbf{S}/2$ ).

For the transitions between the yellow and the blue series, the interband matrix element takes the form

$$\langle \Gamma_6^+, \sigma, \mathbf{q} | e^{-i\mathbf{\kappa} \cdot \mathbf{r}} \boldsymbol{\pi} | \Gamma_8^+, \sigma', \mathbf{q} + \mathbf{\kappa} \rangle = B_{6,8} \mathbf{R}_{\sigma, \sigma'}, \quad (16)$$

where  $B_{6,8}$  is the relevant band structure parameter and  $\mathbf{R}$  is given in Eq. (C6). We fitted the Hamiltonian derived in Appendix C to spin-DFT calculations in the vicinity of the  $\Gamma$ -point<sup>33</sup>, yielding

$$\begin{aligned} A_6 &= 2.44 & A_8 &= 3.99 & A'_8 &= -1.94, \\ A''_8 &= 1.25 & \text{and} & & B_{6,8} &= 0.342 \frac{\hbar\pi}{a_g}. \end{aligned} \quad (17)$$

The resulting band structure is shown in Fig. 3, with excellent agreement to the DFT calculations. Using the effective electron masses as defined in Tab. II yields  $m_e = 0.99 m_0$  for the  $\Gamma_6^+$  conduction band which agrees with the experimental values<sup>34</sup> as well as  $m_e = 0.21 m_0$  for the  $\Gamma_8^-$  conduction band.

#### IV. TRANSITIONS BETWEEN THE YELLOW AND GREEN SERIES IN $\text{Cu}_2\text{O}$

In this section, the transition matrix elements for transitions from the yellow  $P$ -excitons to the green  $S$ - and  $D$ -excitons will be calculated. We will first evaluate them in the dipole approximation of Eq. (9) and subsequently drop the dipole approximation for a representative set of states.

Using the symmetrised basis functions given in Appendix B with hydrogen-like radial wave functions as approximations to the excitonic states, the transition ma-

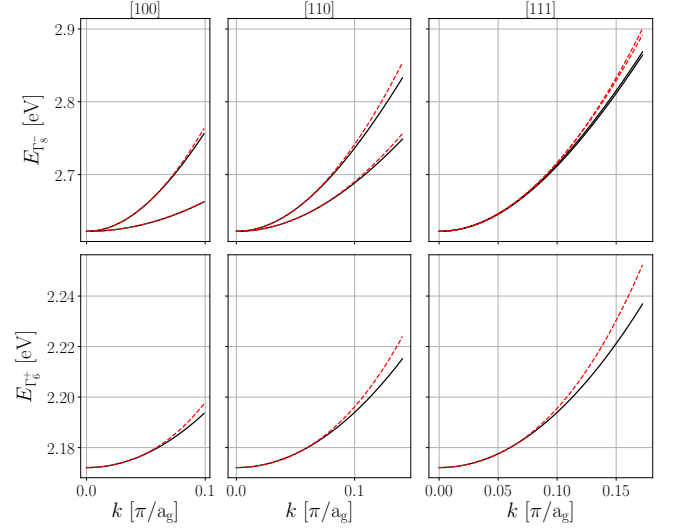


FIG. 3: Conduction band structure of  $\text{Cu}_2\text{O}$ , comparing results from spin-DFT calculations (black solid lines) with fits with the parameters in Eq. (17) (red dashed lines).

trix elements in dipole approximation can now be calculated. Focussing on the transitions from the  $z$ -component of the yellow  $\Gamma_4^-$   $P$ -exciton (without loss of generality), the transition strength to the green  $S$ - and  $D$ -states can be expressed as

$$\sum_i \left| \left\langle Y P_z^{\Gamma_4^-}, n \right| \pi_{x_j} \left| G \ell_i^{\Gamma_6^+}, n' \right\rangle \right|^2 = C_{x_j}^{\Gamma_6^+} |p_r^\ell(n, n')|^2 \quad (18)$$

where the sum over  $i$  runs over the substates of the green  $\ell \Gamma_6^+$ -manifold,  $\ell$  denotes the angular momentum (i.e.  $S$  or  $D$ ) and  $\Gamma_6^+$  the irreducible representations into which the green  $S$ - and  $D$ -excitons can be decomposed. The  $C_{\ell, x_j}^{\Gamma_6^+}$  are listed in Tab. IV and depend only on the spins, the angular momenta as well as the band-structure parameters  $A_2 - B_2$  and  $A_3 - B_3$ . Furthermore,

$$p_r^\ell(n, n') = \hbar \int_0^\infty dk k^3 \tilde{\phi}_{Y P, n}^\dagger(k) \tilde{\phi}_{G \ell, n'}(k) \quad (19)$$

are the radial matrix elements of  $\hbar k$  that are shown in Fig. 4. The representation of Eq. 18 as well as the coefficients can be retrieved by multiplying the symmetrised basis functions in Appendix B with the corresponding transition matrix Eq. (B13) and integrating over the angular coordinates.

In Eq. (19), the sum over  $\mathbf{k}$  has been converted to an integral via  $\sum_{\mathbf{k}} \approx \Omega/(2\pi)^3 \int d^3\mathbf{k}$  with  $\Omega$  the crystal volume. The radial envelope functions  $\tilde{\phi}_\tau(\mathbf{k}) = \sqrt{\Omega/(2\pi)^3} \phi_\tau(\mathbf{k})$  are normalised w.r.t. the integral  $\int d^3\mathbf{k}$ .

In order to include the multipole corrections contained in Eq. (7), we first observe that for interband transitions

TABLE IV: Angular coefficients for dipole transitions into the green  $S$ - and  $D$ -excitons.

$C_{\ell, x_i}^{\Gamma_i^+}$		polarisation $x_i$ ( $\mathbf{e}_2$ )		
		$x$	$y$	$z$
green $S$	$1\Gamma_3^+$	0	0	0.11
	$1\Gamma_4^+$	0.85	0.85	0
	$1\Gamma_5^+$	0.52	0.52	0
	$\Sigma$	1.37	1.37	0.11
green $D$	$2\Gamma_1^+$	0	0	0.47
	$2\Gamma_2^+$	0	0	0
	$3\Gamma_3^+$	0	0	0.87
	$5\Gamma_4^+$	0.41	0.41	0
	$5\Gamma_5^+$	0.44	0.44	0
	$\Sigma$	0.85	0.85	1.34

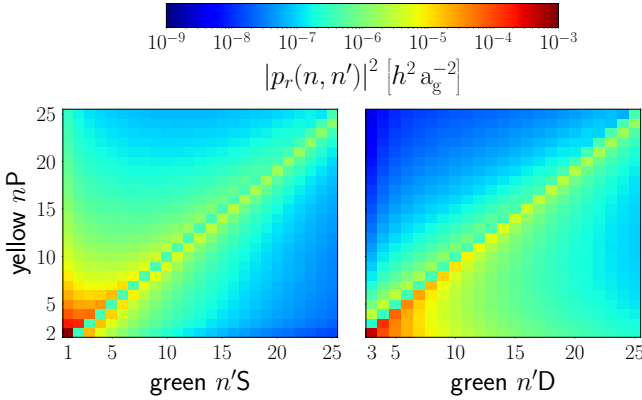


FIG. 4: Radial coefficients as given in Eq. (19). The radial wave functions used are hydrogenic functions with Bohr radii given in Tab. II.

between bands of the same parity, the leading order of the interband matrix element can be expressed as

$$\langle v, -\mathbf{q} - \boldsymbol{\kappa} | e^{-i\boldsymbol{\kappa}\mathbf{r}} \boldsymbol{\pi} | v', -\mathbf{q} \rangle = -\hbar \mathbf{M} \cdot \mathbf{q} - \hbar \mathbf{N} \cdot \boldsymbol{\kappa} \quad (20)$$

with some state-dependent matrices  $\mathbf{M}, \mathbf{N} \in \mathbb{C}^{3 \times 3}$ . In this approximation, Eq. (7) can be rewritten as

$$\begin{aligned} & \left\langle \Psi_{\tau, \mathbf{K}}^{c, v} \left| e^{-i\boldsymbol{\kappa}\mathbf{r}} \boldsymbol{\pi} \right| \Psi_{\tau', \mathbf{K}+\boldsymbol{\kappa}}^{c, v'} \right\rangle \\ &= i \hbar \mathbf{M} \cdot \mathbf{O}(\tau, \tau', (\beta - \beta')\mathbf{K} + \alpha'\boldsymbol{\kappa}) \\ & - \hbar [\mathbf{N} \cdot \boldsymbol{\kappa} - \beta' \mathbf{M} \cdot (\mathbf{K} + \boldsymbol{\kappa})] W(\tau, \tau', (\beta - \beta')\mathbf{K} + \alpha'\boldsymbol{\kappa}) \end{aligned} \quad (21)$$

where

$$\mathbf{O}(\tau, \tau', \mathbf{q}) = \int d^3\mathbf{r} e^{i\mathbf{q}\cdot\mathbf{r}} \phi_{\tau}^{\dagger}(\mathbf{r}) \nabla_{\mathbf{r}} \phi_{\tau'}(\mathbf{r}) \quad (22)$$

TABLE V: Relative transition strengths from  $n_y \Gamma_4^-$   $P$ -excitons to all green  $n_g \Gamma_3^+$ -excitons with both pump and probe beam  $z$ -polarised and propagating along the  $y$ -axis.

$n_y$	$n_g$	co-propagating		counter-propagating	
		$S\Gamma_3^+$	$D\Gamma_3^+$	$S\Gamma_3^+$	$D\Gamma_3^+$
19	20	1.04	0.96	0.76	0.83
14	15	1.02	0.99	0.90	0.94
8	9	1.01	1.00	0.98	0.99

and

$$W(\tau, \tau', \mathbf{q}) = \int d^3\mathbf{r} e^{i\mathbf{q}\cdot\mathbf{r}} \phi_{\tau}^{\dagger}(\mathbf{r}) \phi_{\tau'}(\mathbf{r}) \quad (23)$$

with the real-space (i.e. Fourier transformed) envelope functions  $\phi_{\tau}(\mathbf{r})$ . The integrals  $W(\tau, \tau', \mathbf{q})$  are identical to those appearing in the calculation of the phonon scattering of Rydberg excitons<sup>11</sup>. Table V lists the transition strengths relative to the dipole approximation for some representative transitions from the yellow  $P$ -excitons to the green  $\Gamma_3^+$ -excitons. For counter-propagating beams and a principal quantum number of  $\sim 20$ , the error introduced by the dipole approximation can reach almost 25%.

## V. TRANSITIONS BETWEEN THE YELLOW AND BLUE SERIES IN $\text{Cu}_2\text{O}$

We will now proceed by repeating the analysis of the previous section for transitions from the yellow to the blue  $P$ -excitons. In particular, we will show that the breakdown of the dipole approximation allows transitions to certain blue  $S$ -excitons with transition strengths comparable to those from yellow  $P$  to blue  $P$ -excitons.

The effective mass, averaged spatially as well as over light and heavy holes, of an electron in the  $\Gamma_8^-$  conduction band derived from the fits is  $0.21 m_0$ . Note that some of this mass derives from the coupling to the  $\Gamma_6^+$  conduction band. Hence, this value is not the same as the inverse of  $A_8$  in Eq. (17). As the interband matrix elements are constant to leading order in  $\mathbf{q}$ , the only allowed transitions in the dipole approximation are those between states of the same  $\ell$ . The dipolar transition strengths between yellow  $nP$  and blue  $n'P$  excitons can therefore be written as

$$\begin{aligned} & \sum_i \left| \left\langle YP_z^{\Gamma_4^-}, n \left| \pi_{x_j} \right| BP_i^{\Gamma_3^+}, n' \right\rangle \right|^2 \\ &= |B_{6,8}|^2 D_{P,x_j}^{\Gamma_3^+} |o_r(n, n')|^2 \end{aligned} \quad (24)$$

with the band parameter  $B_{6,8}$  (see Appendix C) and the radial overlap integral

$$o_r(n, n') = \int_0^{\infty} dk k^2 \tilde{\phi}_{YP,n}^{\dagger}(k) \tilde{\phi}_{BP,n'}(k). \quad (25)$$



TABLE VI: Angular coefficients for dipole transitions into the blue  $P$ -excitons.

$D_{P,x_i}^{\Gamma_i^+}$		polarisation $x_i$ ( $\mathbf{e}_2$ )		
		$x$	$y$	$z$
blue P	$1\Gamma_1^+$	0	0	1/3
	$1\Gamma_2^+$	0	0	0
	$2\Gamma_3^+$	0	0	1/3
	$3\Gamma_4^+$	5/12	5/12	0
	$3\Gamma_5^+$	1/4	1/4	0
	$\Sigma$	2/3	2/3	2/3

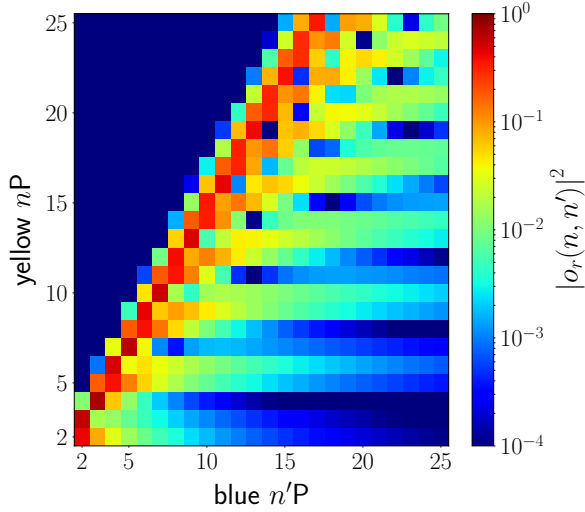


FIG. 5: Radial coefficients as given in Eq. (25) for the transitions between the yellow and blue  $P$ -excitons. The radial wave functions used are hydrogenic functions with Bohr radii given in Tab. II.

The blue  $P$  states have symmetry  $\Gamma_4^- \otimes \Gamma_8^- \otimes \Gamma_7^+ = \Gamma_1^+ \oplus \Gamma_2^+ \oplus 2\Gamma_3^+ \oplus 3\Gamma_4^+ \oplus 3\Gamma_5^+$ , and the corresponding coefficients  $D_{P,x_j}^{\Gamma_j^+}$  are given in Tab. VI with the squared overlap integrals shown in Fig. 5.

For a constant interband transition matrix element  $\langle c, \mathbf{k} | e^{-i\mathbf{\kappa}\mathbf{r}} \boldsymbol{\pi} | c', \mathbf{k} + \boldsymbol{\kappa} \rangle \approx \langle c, 0 | \boldsymbol{\pi} | c', 0 \rangle$ , Eq. (8) can be rewritten as

$$\left\langle \Psi_{\tau, \mathbf{K}}^{c,v} \left| e^{-i\mathbf{\kappa}\mathbf{r}} \boldsymbol{\pi} \right| \Psi_{\tau', \mathbf{K}+\boldsymbol{\kappa}}^{c',v} \right\rangle = \langle c, 0 | \boldsymbol{\pi} | c', 0 \rangle \times W(\tau, \tau', (\alpha' - \alpha)\mathbf{K} - \beta'\boldsymbol{\kappa}). \quad (26)$$

The corrections to transitions from the  $z$ -component of the yellow  $n_y \Gamma_4^-$   $P$ -exciton to all blue  $n_b \Gamma_3^+$   $P$ -states are shown in Fig. 6. The quantity

$$T(n_y, P\Gamma_3^+ n_b; \mathbf{k}, x_j) = |B_{6,8}|^2 \sum_j \left| \left\langle YP_z^{\Gamma_4^-} n_y \left| R_{x_j}^\dagger \otimes \bar{W}(YP n_y, BP n_b, \mathbf{k}) \right| BP_j^{\Gamma_3^+} n_b \right\rangle \right|^2 \quad (27)$$

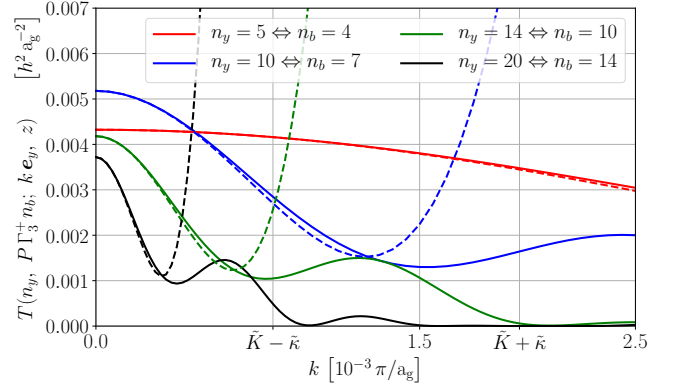


FIG. 6: Transitions from the  $z$ -component of the yellow  $n_y \Gamma_4^-$   $P$ -state to all blue  $n_b \Gamma_3^+$   $P$ -states via a  $z$ -polarised probe beam. The dashed lines indicate the sum of the dipole and octupole contributions.

shown there coincides with the exact transition strength for  $\mathbf{k} = (\alpha' - \alpha)\mathbf{K} - \beta'\boldsymbol{\kappa}$  and with the dipole approximation for  $\mathbf{k} = 0$ . Here,  $j$  sums over all four sub-states of the two  $\Gamma_3^+$  representations appearing in the decomposition of the blue  $P$ -excitons (see Tab. VI),  $\bar{W}(\tau, \tau', \mathbf{k}) \in \mathbb{C}^{(2\ell+1) \times (2\ell'+1)}$  denotes the matrix containing the  $W(\tau, \tau', \mathbf{k})$  for all combinations of magnetic quantum numbers, the  $R_{x_j}$  are the interband coefficient matrices given in Eq. (C6), and  $|BP_j^{\Gamma_3^+} n_b\rangle$  as well as  $|YP_z^{\Gamma_4^-} n_y\rangle$  are the symmetrised basis states of App. B.

For the given relative electron masses in  $\text{Cu}_2\text{O}$ , the scaled COM wavenumber of the yellow exciton is  $\tilde{K} = (\alpha - \alpha')|\mathbf{K}| = 1.39 \times 10^{-3} \pi a_g^{-1}$ , and  $\tilde{\kappa} = \beta'|\boldsymbol{\kappa}| = 0.57 \times 10^{-3} \pi a_g^{-1}$  is the photon wavenumber scaled by the relative hole mass of the blue exciton. These values have been calculated from the band gaps of the yellow and blue series and should be accurate to within 1% even for the  $n_y = 5 \leftrightarrow n_b = 4$  transition. The sum  $\tilde{K} + \tilde{\kappa}$  appears for co-propagating beams and the difference  $\tilde{K} - \tilde{\kappa}$  for counter-propagating beams (see Tab. III).

There is a prominent effect from the abandonment of the dipole approximation even for principal quantum numbers  $n_y \approx 5$ . In Fig. 6, the dashed lines show the sum of dipole and octupole contributions only, which deviates strongly from the exact result (solid lines) for larger momentum transfer  $k$ . However, the deviation of the exact result from the low-order multipole expansion is least for counter-propagating beams. In Fig. 7, we show the transition strengths from the yellow  $\Gamma_4^-$   $P$ -excitons to the blue  $\Gamma_3^-$   $S$ -excitons which are usually dipole-forbidden. Hence, the first non-vanishing contribution is that of a quadrupole interaction. Note that the magnitudes of the transition matrix elements are of the same order of magnitude as in Fig. 6.

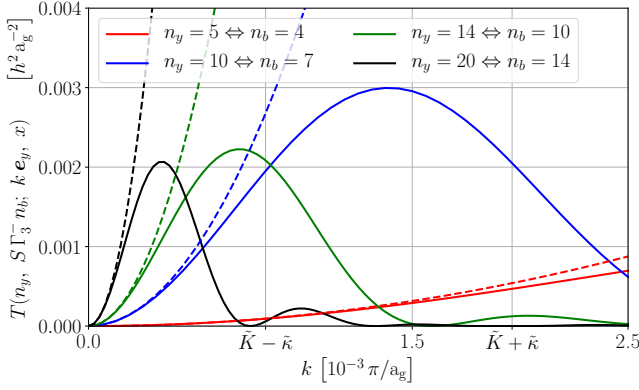


FIG. 7: Same as Fig. 6 for the transition to the blue  $\Gamma_3^-$   $S$ -excitons via  $x$ -polarised probe beams. Dashed lines indicate the quadrupole approximation.

## VI. DISCUSSION AND OUTLOOK

We have presented detailed calculations for the transition strengths of the excitonic interseries transitions in  $\text{Cu}_2\text{O}$ , going well beyond the dipole approximation. Those transitions can either be between the yellow and green series, where the hole changes the valence band, or between the yellow and blue series with an accompanying change of the conduction band. The symmetry properties of the respective bands imply that dipole transitions are only allowed for  $|\Delta\ell| = 1$  (yellow-green) or  $\Delta\ell = 0$  (yellow-blue), respectively.

Transitions between Rydberg excitons of different series are located at wavelengths that are comparable with the size of the Rydberg wavefunctions. Hence, the dipole approximation is no longer valid, and the inclusion of multipoles of all orders is necessary. We have shown that, already for relatively low principal quantum numbers, the deviation from the dipole approximation cannot be neglected. In particular, dipole-forbidden transitions such as from yellow  $P$ -excitons to blue  $S$ -excitons become allowed to the extent that their transition matrix elements are of similar size to those of dipole-allowed transitions. These results pave the way to construct protocols for coherent manipulation of Rydberg excitons.

So far, our calculations are based on the exciton parameters collected in Tab. II which were derived from band-structure parameters of  $\text{Cu}_2\text{O}$  and show discrepancies to the experimental data. To improve on these, a detailed theory of the green<sup>35,36</sup> and blue Rydberg excitons, including the coupling to the yellow continuum states, would be necessary. Furthermore, both the  $\Gamma_8^+$  valence band and the  $\Gamma_8^-$  conduction band have an anisotropic mass at the  $\Gamma$ -point that will result in a strong coupling of different angular momenta even for Rydberg states and a corresponding redistribution of the transition strengths over more states than we have taken into account so far. To the best of our knowledge, no experiments have been performed, from which the excitonic interseries transition

strengths in  $\text{Cu}_2\text{O}$  could be quantified.

Proposals have been put forward to use spatially modulated light fields such as orbital angular momentum (OAM) light in order to tune the selection rules of excitonic transitions<sup>37</sup>. Realising such transitions is, however, experimentally challenging as the real-space extension of both initial and final states has to be comparable to the characteristic length scale of the modulation, or the transversal position inside the beam has to be controlled very precisely<sup>38,39</sup>. Excitonic interseries transitions, on the other hand, have the advantage that both initial and final states can in principle become arbitrarily large while the energy separation, and hence the wavelength of the coupling beam, approaches a finite value. This work paves the way towards the evaluation of such transition matrix elements which we leave for a future publication.

## Acknowledgments

We would like to thank Dr. Martin French for providing us with the high-resolution SDFIT calculations of the conduction bands in the vicinity of the  $\Gamma$ -point. We gratefully acknowledge support by the DFG SPP 1929 GiRyd.

## Appendix A: Interband matrix elements

The Suzuki–Hensel Hamiltonian in the  $\Gamma_7^+ - \Gamma_8^+$  cross space represents the perturbation theoretical  $\mathbf{k} \cdot \boldsymbol{\pi}$ -Hamiltonian of the form<sup>40</sup>

$$[\mathcal{H}_{\mathbf{q}} + \mathcal{H}_{\mathbf{B}}]_{\sigma, \sigma'} = \frac{\hbar^2}{2m_0^2} \sum_n \Delta_n^{-1} \times \langle u_{\Gamma_7^+}, \sigma, 0 | \mathbf{q} \cdot \boldsymbol{\pi} | u_n, 0 \rangle \langle u_n, 0 | \mathbf{q} \cdot \boldsymbol{\pi} | u_{\Gamma_8^+}, \sigma', 0 \rangle + \mathcal{O}(q^4) \quad (\text{A1})$$

where

$$\Delta_n^{-1} = \frac{1}{E_{\Gamma_8^+}(0) - E_n(0)} + \frac{1}{E_{\Gamma_7^+}(0) - E_n(0)}, \quad (\text{A2})$$

$\mathcal{H}_{\mathbf{q}}$  denotes only the  $\mathbf{q}$ -dependent part of  $\mathcal{H}(\mathbf{q})$ , and the magnetic field  $\mathbf{B}$  is given by the commutator<sup>32,41</sup>

$$\mathbf{q} \times \mathbf{q} = \frac{e\mathbf{B}}{i\hbar}. \quad (\text{A3})$$

In this notation,  $\sigma = \{\pm 1/2\}$  and  $\sigma' = \{\pm 1/2, \pm 3/2\}$  denote the valence band “spin”. The representations  $\Gamma_7^+$  and  $\Gamma_8^+$  are left out for notational convenience but are nonetheless implied. For a vanishing magnetic field one obtains

$$[\mathcal{H}_{\mathbf{q}}]_{\sigma, \sigma'} = \frac{\hbar \mathbf{q}}{2m_0} \cdot \langle u_{\Gamma_7^+}, \sigma, \mathbf{q} | \boldsymbol{\pi} | u_{\Gamma_8^+}, \sigma', \mathbf{q} \rangle \quad (\text{A4})$$



as can be seen from Eq. (12). This can be rewritten as

$$[\mathcal{H}_{\mathbf{q}}]_{\sigma,\sigma'} = \frac{\hbar^2}{2m_0} \mathbf{q} \cdot \mathbf{M}_{\sigma,\sigma'} \cdot \mathbf{q} \quad (\text{A5})$$

and

$$\langle u_{\Gamma_7^+}, \sigma, \mathbf{q} | \pi | u_{\Gamma_8^+}, \sigma', \mathbf{q} \rangle = \hbar \mathbf{M}_{\sigma,\sigma'} \cdot \mathbf{q} \quad (\text{A6})$$

with some state-dependent matrix  $\mathbf{M}_{\sigma,\sigma'} \in \mathbb{C}^{3 \times 3}$ . For a symmetric matrix  $\mathbf{M}_{\sigma,\sigma'}$  it follows that  $\nabla_{\mathbf{q}}(\mathbf{q} \cdot \mathbf{M}_{\sigma,\sigma'} \cdot \mathbf{q}) = 2\mathbf{M}_{\sigma,\sigma'} \cdot \mathbf{q}$ , which would imply

$$\begin{aligned} \langle u_{\Gamma_7^+}, \sigma, \mathbf{q} | \pi | u_{\Gamma_8^+}, \sigma', \mathbf{q} \rangle &= m_0 \hbar^{-1} \nabla_{\mathbf{q}} [\mathcal{H}_{\mathbf{q}}]_{\sigma,\sigma'} \\ &= m_0 \hbar^{-1} \nabla_{\mathbf{q}} [\mathcal{H}(\mathbf{q})]_{\sigma,\sigma'}. \end{aligned} \quad (\text{A7})$$

All that is left to show is hence, that the  $\mathbf{M}$  are indeed symmetric matrices. Their components can be written as

$$\begin{aligned} &\mathbf{M}_{\sigma,\sigma'}^{x_i, x_j} \\ &= \frac{1}{m_0} \sum_n \frac{\langle u_{\Gamma_7^+}, \sigma, 0 | \pi_{x_j} | u_n, 0 \rangle \langle u_n, 0 | \pi_{x_i} | u_{\Gamma_8^+}, \sigma', 0 \rangle}{E_{\Gamma_7^+}(0) - E_n(0)} \\ &+ \frac{1}{m_0} \sum_n \frac{\langle u_{\Gamma_7^+}, \sigma, 0 | \pi_{x_i} | u_n, 0 \rangle \langle u_n, 0 | \pi_{x_j} | u_{\Gamma_8^+}, \sigma', 0 \rangle}{E_{\Gamma_8^+}(0) - E_n(0)}. \end{aligned} \quad (\text{A8})$$

They are obviously symmetric w.r.t. an exchange of  $x_i$  and  $x_j$  under the approximation that the two energy denominators are equal. Again, this approximation is reasonable as the next possible coupling states  $|u_n, 0\rangle$  (of  $\Gamma_7^-$  or  $\Gamma_8^-$  symmetry) are removed by about  $20\Delta_{so}$ . The components of  $m_0 \hbar^{-1} \nabla_{\mathbf{q}} \mathcal{H}(\mathbf{q})$  are then given by  $\hbar \mathbf{M}_{\sigma,\sigma'} \cdot \mathbf{q}$  where the  $\mathbf{M}$  are defined by

$$\mathbf{M}_{\sigma,\sigma'} = \begin{pmatrix} \langle \Gamma_7^+, -1/2 | & \langle \Gamma_7^+, 1/2 | \\ \mathbf{M}_{5,z} & \mathbf{M}_{3,1} \\ \mathbf{M}_{3,2} + \mathbf{M}_{5,xy} & \sqrt{\frac{1}{3}} \mathbf{M}_{5,z} \\ \sqrt{\frac{1}{3}} \mathbf{M}_{5,z}^\dagger & -\mathbf{M}_{3,2} + \mathbf{M}_{5,xy} \\ -\mathbf{M}_{3,1} & \mathbf{M}_{5,z}^\dagger \end{pmatrix} \begin{pmatrix} | \Gamma_8^+, -3/2 \rangle \\ | \Gamma_8^+, -1/2 \rangle \\ | \Gamma_8^+, 1/2 \rangle \\ | \Gamma_8^+, 3/2 \rangle \end{pmatrix} \quad (\text{A9})$$

with

$$\mathbf{M}_{5,z} = \frac{A_3 - B_3}{\sqrt{8}} \begin{pmatrix} 0 & 0 & 1 \\ 0 & 0 & i \\ 1 & i & 0 \end{pmatrix}, \quad (\text{A10})$$

$$\mathbf{M}_{3,1} = \frac{A_2 - B_2}{\sqrt{18}} \begin{pmatrix} -1 & 0 & 0 \\ 0 & -1 & 0 \\ 0 & 0 & 2 \end{pmatrix}, \quad (\text{A11})$$

$$\mathbf{M}_{3,2} = \frac{A_2 - B_2}{\sqrt{6}} \begin{pmatrix} 1 & 0 & 0 \\ 0 & -1 & 0 \\ 0 & 0 & 0 \end{pmatrix}, \quad (\text{A12})$$

and

$$\mathbf{M}_{5,xy} = \frac{A_3 - B_3}{\sqrt{6}} \begin{pmatrix} 0 & i & 0 \\ i & 0 & 0 \\ 0 & 0 & 0 \end{pmatrix}. \quad (\text{A13})$$

Under the same approximations, the  $\kappa$ -dependent part of Eq. (12) can be rewritten as

$$\begin{aligned} &\frac{\hbar}{m_0} \sum_n \frac{\langle u_{\Gamma_7^+}, \sigma, 0 | \kappa \cdot \pi | u_n, 0 \rangle \langle u_n, 0 | \pi | u_{\Gamma_8^+}, \sigma', 0 \rangle}{E_{\Gamma_7^+}(0) - E_n(0)} \\ &= \frac{m_0}{2\hbar} \nabla_{\kappa} [\mathcal{H}(\kappa)]_{\sigma,\sigma'} + F \tilde{\mathbf{N}}_{\sigma,\sigma'} \cdot \hbar \kappa \end{aligned} \quad (\text{A14})$$

where  $\tilde{\mathbf{N}}_{\sigma,\sigma'} = (\mathbf{N}_{\sigma,\sigma'} - \mathbf{N}_{\sigma,\sigma'}^T)/2$  is the antisymmetric part of

$$\begin{aligned} &\mathbf{N}_{\sigma,\sigma'}^{x_i, x_j} = \\ &\frac{1}{F m_0} \sum_n \frac{\langle u_{\Gamma_7^+}, \sigma, 0 | \pi_{x_j} | u_n, 0 \rangle \langle u_n, 0 | \pi_{x_i} | u_{\Gamma_8^+}, \sigma', 0 \rangle}{E_{\Gamma_7^+}(0) - E_n(0)} \end{aligned} \quad (\text{A15})$$

and  $F$  is an additional parameter. We thus arrive at

$$\begin{aligned} &\langle u_{\Gamma_7^+}, \sigma, \mathbf{q} + \kappa | \pi | u_{\Gamma_8^+}, \sigma', \mathbf{q} + \kappa \rangle \\ &= \frac{m_0}{\hbar} \nabla_{\mathbf{q} + \frac{\kappa}{2}} \left[ \mathcal{H} \left( \mathbf{q} + \frac{\kappa}{2} \right) \right]_{\sigma,\sigma'} + F \tilde{\mathbf{N}}_{\sigma,\sigma'} \cdot \hbar \kappa. \end{aligned} \quad (\text{A16})$$

The matrices  $\tilde{\mathbf{N}}$  for all state combinations can be calculated by the applying the Wigner-Eckart theorem of  $O_h$  to Eq. (A15) and a subsequent antisymmetrisation which results in

$$\tilde{\mathbf{N}}_{\sigma,\sigma'} = \begin{pmatrix} \langle \Gamma_7^+, -1/2 | & \langle \Gamma_7^+, 1/2 | \\ \sqrt{\frac{1}{3}} \tilde{\mathbf{N}}_{4,xy} & \tilde{\mathbf{N}}_{4,z} \\ 0 & -\tilde{\mathbf{N}}_{4,xy} \\ -\tilde{\mathbf{N}}_{4,xy}^* & 0 \\ \tilde{\mathbf{N}}_{4,z} & \sqrt{\frac{1}{3}} \tilde{\mathbf{N}}_{4,xy}^* \end{pmatrix} \begin{pmatrix} | \Gamma_8^+, -3/2 \rangle \\ | \Gamma_8^+, -1/2 \rangle \\ | \Gamma_8^+, 1/2 \rangle \\ | \Gamma_8^+, 3/2 \rangle \end{pmatrix} \quad (\text{A17})$$

where the  $*$  denotes a complex conjugation and

$$\tilde{\mathbf{N}}_{4,xy} = \sqrt{\frac{1}{2}} \begin{pmatrix} 0 & 0 & -1 \\ 0 & 0 & -i \\ 1 & i & 0 \end{pmatrix} \quad (\text{A18})$$

as well as

$$\tilde{\mathbf{N}}_{4,z} = \sqrt{\frac{2}{3}} \begin{pmatrix} 0 & i & 0 \\ -i & 0 & 0 \\ 0 & 0 & 0 \end{pmatrix}. \quad (\text{A19})$$

Due to the antisymmetry of  $\tilde{\mathbf{N}}$ , one can rewrite  $\boldsymbol{\kappa} \cdot \tilde{\mathbf{N}}_{\sigma,\sigma'} \cdot \boldsymbol{\kappa} = e/(i\hbar) \mathbf{v}_{\sigma,\sigma'} \cdot \mathbf{B}$  where

$$\mathbf{v}_{4,xy} = \sqrt{\frac{1}{2}} \begin{pmatrix} -i \\ 1 \\ 0 \end{pmatrix}, \quad \mathbf{v}_{4,z} = \sqrt{\frac{2}{3}} \begin{pmatrix} 0 \\ 0 \\ i \end{pmatrix} \quad (\text{A20})$$

and the commutation relation in Eq. (A3) has been used. This tells us that the parameter  $F$  is related to the magnetic part of the valence-band Hamiltonian which is given by (ignoring spin-orbit terms)<sup>32</sup>

$$\mathcal{H}_{\mathbf{B}} = \frac{\hbar e}{m_0} [A_4 \mathbf{I} + B_4 \mathbf{S}] \cdot \mathbf{B}. \quad (\text{A21})$$

Inserting  $[E_{\Gamma_7^+}(0) - E_n(0)]^{-1} \approx \Delta_n^{-1}/2$  into Eq. (A14), we can thus write

$$\begin{aligned} \frac{\hbar^2 F}{2m_0} \boldsymbol{\kappa} \cdot \tilde{\mathbf{N}}_{\sigma,\sigma'} \cdot \boldsymbol{\kappa} &= \frac{1}{2} [\mathcal{H}_{\mathbf{B}}]_{\sigma,\sigma'} \\ \Rightarrow \frac{\hbar e}{2m_0} F \frac{\mathbf{v}_{\sigma,\sigma'}}{i} \cdot \mathbf{B} &= \frac{\hbar e}{2m_0} [A_4 \mathbf{I}_{\sigma,\sigma'} + B_4 \mathbf{S}_{\sigma,\sigma'}] \cdot \mathbf{B} \end{aligned} \quad (\text{A22})$$

and find by comparison  $F = -(A_4 - 2B_4)/\sqrt{3}$ . A further comparison with the magnetic valence-band Hamiltonian

$$\mathcal{H}_{\mathbf{B}} = \frac{\hbar e}{m_0} \left[ \left( \frac{3\kappa}{2} + \frac{g_s}{4} \right) \mathbf{I} - \frac{g_s}{4} \mathbf{S} \right] \cdot \mathbf{B} \quad (\text{A23})$$

and its parameters given in Ref.<sup>12</sup> yields

$$F = -\sqrt{\frac{3}{4}} \left( \kappa + \frac{g_s}{2} \right) \approx -0.43 \quad (\text{A24})$$

where  $g_s \approx 2$  and  $\kappa \approx -0.5$  is the fourth Luttinger parameter<sup>41</sup>. Note that the spin matrices are defined differently there,  $\mathbf{I}$  differs by a factor of  $\hbar$  and  $\mathbf{S}_h = \hbar \mathbf{S}/2$ . For the transition between Rydberg excitons of different parity, the term in Eq. (A14) will be small compared to both the transition strength and the correction from the displacement of the momentum-space envelope functions in Eq. (7).

In the case of transitions between the yellow and blue series, the matrix elements of the  $\Gamma_6^+$  and  $\Gamma_8^-$  conduction bands are of interest. Transitions between these bands are allowed at the  $\Gamma$ -point and the band Hamiltonian thus takes the form

$$[\mathcal{H}_{\mathbf{q}}]_{\sigma,\sigma'} = \frac{\hbar}{m_0} \langle u_{\Gamma_6^+}, \sigma, 0 | \mathbf{q} \cdot \boldsymbol{\pi} | u_{\Gamma_8^-}, \sigma', 0 \rangle + \mathcal{O}(q^3) \quad (\text{A25})$$

which is equivalent to Eq. (C5) and directly contains the sought after transition matrix elements via

$$\begin{aligned} \langle u_{\Gamma_6^+}, \sigma, \mathbf{q} | \boldsymbol{\pi} | u_{\Gamma_8^-}, \sigma', \mathbf{q} + \boldsymbol{\kappa} \rangle &= \frac{m_0}{\hbar} \nabla_{\mathbf{q}} [\mathcal{H}_{\mathbf{q}}]_{\sigma,\sigma'} \\ &= \frac{m_0}{\hbar} \nabla_{\mathbf{q}} [\mathcal{H}(\mathbf{q})]_{\sigma,\sigma'} = \langle u_{\Gamma_6^+}, \sigma, 0 | \boldsymbol{\pi} | u_{\Gamma_8^-}, \sigma', 0 \rangle. \end{aligned} \quad (\text{A26})$$

The next higher-order terms would be of order  $q^2$  and  $q\kappa$ .

## Appendix B: Symmetrised basis states

Here we list the symmetrised basis states for the yellow  $\Gamma_4^-$   $P$ -excitons and the green  $S$ - and  $D$ -excitons which are equivalent to the one used in Ref.<sup>31</sup>. Note, that all following states are constructed in terms of valence band holes. The product states of the bands forming the yellow series give  $\Gamma_7^+ \otimes \Gamma_6^+ = \Gamma_2^+ \oplus \Gamma_5^+$  where<sup>42</sup>

$$Y^{\Gamma_2^+} = \sqrt{\frac{1}{2}} \left( \psi_{1/2}^{\Gamma_6^+} \psi_{-1/2}^{\Gamma_7^+} - \psi_{-1/2}^{\Gamma_6^+} \psi_{1/2}^{\Gamma_7^+} \right), \quad (\text{B1})$$

$$Y_{yz}^{\Gamma_5^+} = i\sqrt{\frac{1}{2}} \left( \psi_{1/2}^{\Gamma_6^+} \psi_{1/2}^{\Gamma_7^+} - \psi_{-1/2}^{\Gamma_6^+} \psi_{-1/2}^{\Gamma_7^+} \right), \quad (\text{B2})$$

$$Y_{zx}^{\Gamma_5^+} = \sqrt{\frac{1}{2}} \left( \psi_{1/2}^{\Gamma_6^+} \psi_{1/2}^{\Gamma_7^+} + \psi_{-1/2}^{\Gamma_6^+} \psi_{-1/2}^{\Gamma_7^+} \right), \quad (\text{B3})$$

$$Y_{xy}^{\Gamma_5^+} = -i\sqrt{\frac{1}{2}} \left( \psi_{1/2}^{\Gamma_6^+} \psi_{-1/2}^{\Gamma_7^+} + \psi_{-1/2}^{\Gamma_6^+} \psi_{1/2}^{\Gamma_7^+} \right). \quad (\text{B4})$$

In the same vein, the states of the green series can be expressed as  $\Gamma_8^+ \otimes \Gamma_6^+ = \Gamma_3^+ \oplus \Gamma_4^+ \oplus \Gamma_5^+$

$$G_1^{\Gamma_3^+} = -\sqrt{\frac{1}{2}} \left( \psi_{1/2}^{\Gamma_6^+} \psi_{-1/2}^{\Gamma_8^+} + \psi_{-1/2}^{\Gamma_6^+} \psi_{1/2}^{\Gamma_8^+} \right), \quad (\text{B5})$$

$$G_2^{\Gamma_3^+} = -\sqrt{\frac{1}{2}} \left( \psi_{1/2}^{\Gamma_6^+} \psi_{3/2}^{\Gamma_8^+} + \psi_{-1/2}^{\Gamma_6^+} \psi_{-3/2}^{\Gamma_8^+} \right), \quad (\text{B6})$$

$$\begin{aligned} G_x^{\Gamma_4^+} &= i\sqrt{\frac{1}{8}} \left( \sqrt{3} \left[ \psi_{-1/2}^{\Gamma_6^+} \psi_{3/2}^{\Gamma_8^+} + \psi_{1/2}^{\Gamma_6^+} \psi_{-3/2}^{\Gamma_8^+} \right] \right. \\ &\quad \left. - \left[ \psi_{-1/2}^{\Gamma_6^+} \psi_{-1/2}^{\Gamma_8^+} + \psi_{1/2}^{\Gamma_6^+} \psi_{1/2}^{\Gamma_8^+} \right] \right), \end{aligned} \quad (\text{B7})$$

$$\begin{aligned} G_y^{\Gamma_4^+} &= \sqrt{\frac{1}{8}} \left( \sqrt{3} \left[ \psi_{-1/2}^{\Gamma_6^+} \psi_{3/2}^{\Gamma_8^+} - \psi_{1/2}^{\Gamma_6^+} \psi_{-3/2}^{\Gamma_8^+} \right] \right. \\ &\quad \left. + \left[ \psi_{-1/2}^{\Gamma_6^+} \psi_{-1/2}^{\Gamma_8^+} - \psi_{1/2}^{\Gamma_6^+} \psi_{1/2}^{\Gamma_8^+} \right] \right), \end{aligned} \quad (\text{B8})$$

$$G_z^{\Gamma_4^+} = i\sqrt{\frac{1}{2}} \left( \psi_{1/2}^{\Gamma_6^+} \psi_{-1/2}^{\Gamma_8^+} - \psi_{-1/2}^{\Gamma_6^+} \psi_{1/2}^{\Gamma_8^+} \right), \quad (\text{B9})$$

$$G_{yz}^{\Gamma_5^+} = -i\sqrt{\frac{1}{8}} \left( \left[ \psi_{-1/2}^{\Gamma_6^+} \psi_{3/2}^{\Gamma_8^+} + \psi_{1/2}^{\Gamma_6^+} \psi_{-3/2}^{\Gamma_8^+} \right] + \sqrt{3} \left[ \psi_{-1/2}^{\Gamma_6^+} \psi_{-1/2}^{\Gamma_8^+} + \psi_{1/2}^{\Gamma_6^+} \psi_{1/2}^{\Gamma_8^+} \right] \right), \quad (\text{B10})$$

$$G_{zx}^{\Gamma_5^+} = \sqrt{\frac{1}{8}} \left( \left[ \psi_{-1/2}^{\Gamma_6^+} \psi_{3/2}^{\Gamma_8^+} - \psi_{1/2}^{\Gamma_6^+} \psi_{-3/2}^{\Gamma_8^+} \right] - \sqrt{3} \left[ \psi_{-1/2}^{\Gamma_6^+} \psi_{-1/2}^{\Gamma_8^+} - \psi_{1/2}^{\Gamma_6^+} \psi_{1/2}^{\Gamma_8^+} \right] \right), \quad (\text{B11})$$

$$G_{xy}^{\Gamma_5^+} = i\sqrt{\frac{1}{2}} \left( \psi_{1/2}^{\Gamma_6^+} \psi_{3/2}^{\Gamma_8^+} - \psi_{-1/2}^{\Gamma_6^+} \psi_{-3/2}^{\Gamma_8^+} \right). \quad (\text{B12})$$

The valence-band transition matrix of Eq. (A16) in the 12-dimensional spinor-space of  $\Gamma_6^+ \otimes (\Gamma_7^+ \oplus \Gamma_8^+)$  is simply

$$\left[ \frac{m_0}{\hbar} \nabla_{\mathbf{q} + \frac{\kappa}{2}} \left[ \mathcal{H} \left( \mathbf{q} + \frac{\kappa}{2} \right) \right]_{\sigma, \sigma'} + F \hbar \tilde{\mathbf{N}} \cdot \boldsymbol{\kappa} \right] \otimes \text{Id}_6 \quad (\text{B13})$$

where  $\text{Id}_6$  is the unity operator in the  $\Gamma_6^+$ -Hilbert space of the conduction band. The yellow  $\Gamma_4^-$   $P$ -excitons can then be constructed with the cubic harmonics<sup>43</sup> for  $\ell = 1$

$$\xi_x^{1, \Gamma_4^-} = \frac{Y_1^{-1} - Y_1^1}{\sqrt{2}}, \quad \xi_y^{1, \Gamma_4^-} = i \frac{Y_1^{-1} + Y_1^1}{\sqrt{2}}, \quad \xi_z^{1, \Gamma_4^-} = Y_1^0 \quad (\text{B14})$$

as

$$Y P_x^{\Gamma_4^-} = \frac{\phi}{\sqrt{2}} \left( i Y_{xy}^{\Gamma_5^+} \frac{Y_1^{-1} + Y_1^1}{\sqrt{2}} + Y_{zx}^{\Gamma_5^+} Y_1^0 \right), \quad (\text{B15})$$

$$Y P_y^{\Gamma_4^-} = \frac{\phi}{\sqrt{2}} \left( Y_{xy}^{\Gamma_5^+} \frac{Y_1^{-1} - Y_1^1}{\sqrt{2}} + Y_{yz}^{\Gamma_5^+} Y_1^0 \right), \quad (\text{B16})$$

$$Y P_z^{\Gamma_4^-} = \frac{\phi}{2} \left( Y_{zx}^{\Gamma_5^+} [Y_1^{-1} - Y_1^1] + i Y_{yz}^{\Gamma_5^+} [Y_1^{-1} + Y_1^1] \right), \quad (\text{B17})$$

where the  $Y_\ell^m$  are the spherical harmonics and  $\phi$  denotes the radial wave function which is assumed to depend only on  $n, \ell$  and the excitonic series (i.e. yellow, green or blue).

The green  $S$ -states can be constructed by multiplying each of the product states in Eqs. (B5)–(B12) by  $\phi Y_0^0$ . There are 40 green  $D$ -states in total, which will not be listed here but can easily be constructed with the coupling constants given in Ref.<sup>42</sup> and the cubic harmonics for  $\ell = 2$ :

$$\begin{aligned} \xi_1^{2, \Gamma_3^+} &= Y_2^0, & \xi_2^{2, \Gamma_3^+} &= \frac{Y_2^{-2} + Y_2^2}{\sqrt{2}}, \\ \xi_{yz}^{2, \Gamma_5^+} &= i \frac{Y_2^{-1} + Y_2^1}{\sqrt{2}}, & \xi_{zx}^{2, \Gamma_5^+} &= \frac{Y_2^{-1} - Y_2^1}{\sqrt{2}}, \\ \xi_{xy}^{2, \Gamma_5^+} &= i \frac{Y_2^{-2} - Y_2^2}{\sqrt{2}}. \end{aligned} \quad (\text{B18})$$

The blue product states form  $\Gamma_8^- \otimes \Gamma_7^+ = \Gamma_3^- \oplus \Gamma_4^- \oplus \Gamma_5^-$

where

$$B_1^{\Gamma_3^-} = -\sqrt{\frac{1}{2}} \left( \psi_{-1/2}^{\Gamma_7^+} \psi_{-3/2}^{\Gamma_8^-} + \psi_{1/2}^{\Gamma_7^+} \psi_{3/2}^{\Gamma_8^-} \right), \quad (\text{B19})$$

$$B_2^{\Gamma_3^-} = \sqrt{\frac{1}{2}} \left( \psi_{-1/2}^{\Gamma_7^+} \psi_{1/2}^{\Gamma_8^-} + \psi_{1/2}^{\Gamma_7^+} \psi_{-1/2}^{\Gamma_8^-} \right), \quad (\text{B20})$$

$$B_x^{\Gamma_4^-} = -i\sqrt{\frac{1}{8}} \left( \sqrt{3} \left[ \psi_{-1/2}^{\Gamma_7^+} \psi_{-1/2}^{\Gamma_8^-} + \psi_{1/2}^{\Gamma_7^+} \psi_{1/2}^{\Gamma_8^-} \right] + \left[ \psi_{-1/2}^{\Gamma_7^+} \psi_{3/2}^{\Gamma_8^-} + \psi_{1/2}^{\Gamma_7^+} \psi_{-3/2}^{\Gamma_8^-} \right] \right), \quad (\text{B21})$$

$$B_y^{\Gamma_4^-} = \sqrt{\frac{1}{8}} \left( \sqrt{3} \left[ \psi_{1/2}^{\Gamma_7^+} \psi_{1/2}^{\Gamma_8^-} - \psi_{-1/2}^{\Gamma_7^+} \psi_{-1/2}^{\Gamma_8^-} \right] + \left[ \psi_{-1/2}^{\Gamma_7^+} \psi_{3/2}^{\Gamma_8^-} - \psi_{1/2}^{\Gamma_7^+} \psi_{-3/2}^{\Gamma_8^-} \right] \right), \quad (\text{B22})$$

$$B_z^{\Gamma_4^-} = i\sqrt{\frac{1}{2}} \left( \psi_{1/2}^{\Gamma_7^+} \psi_{3/2}^{\Gamma_8^-} - \psi_{-1/2}^{\Gamma_7^+} \psi_{-3/2}^{\Gamma_8^-} \right), \quad (\text{B23})$$

$$B_{yz}^{\Gamma_5^-} = -i\sqrt{\frac{1}{8}} \left( \left[ \psi_{-1/2}^{\Gamma_7^+} \psi_{-1/2}^{\Gamma_8^-} + \psi_{1/2}^{\Gamma_7^+} \psi_{1/2}^{\Gamma_8^-} \right] - \sqrt{3} \left[ \psi_{-1/2}^{\Gamma_7^+} \psi_{3/2}^{\Gamma_8^-} + \psi_{1/2}^{\Gamma_7^+} \psi_{-3/2}^{\Gamma_8^-} \right] \right), \quad (\text{B24})$$

$$B_{zx}^{\Gamma_5^-} = \sqrt{\frac{1}{8}} \left( \left[ \psi_{-1/2}^{\Gamma_7^+} \psi_{-1/2}^{\Gamma_8^-} - \psi_{1/2}^{\Gamma_7^+} \psi_{1/2}^{\Gamma_8^-} \right] + \sqrt{3} \left[ \psi_{-1/2}^{\Gamma_7^+} \psi_{3/2}^{\Gamma_8^-} - \psi_{1/2}^{\Gamma_7^+} \psi_{-3/2}^{\Gamma_8^-} \right] \right), \quad (\text{B25})$$

$$B_{xy}^{\Gamma_5^-} = i\sqrt{\frac{1}{2}} \left( \psi_{1/2}^{\Gamma_7^+} \psi_{-1/2}^{\Gamma_8^-} - \psi_{-1/2}^{\Gamma_7^+} \psi_{1/2}^{\Gamma_8^-} \right). \quad (\text{B26})$$

There are 24 blue  $P$ -states, which can be constructed in the same manner from these product states and the coupling coefficients given by Koster<sup>42</sup>. The interband matrix for transitions between the yellow and blue series can be expressed as  $\text{Id}_7 \otimes [B_{6,s} \mathbf{R}]$ .

### Appendix C: Conduction-band Hamiltonian

In order to describe the transitions between the yellow and the blue series, a band Hamiltonian describing the  $\Gamma_6^+$  and  $\Gamma_8^-$  conduction bands is needed (or at least the offdiagonal part thereof). For the  $\Gamma_6^+$ -subspace there is one free parameter for the terms of zeroth order in  $\mathbf{q}$  ( $\hat{=}\Gamma_1^+$ ) and one parameter for the terms of second order ( $\hat{=}\Gamma_4^- \otimes \Gamma_4^- = \Gamma_1^+ \oplus \Gamma_3^+ \oplus \Gamma_4^+ \oplus \Gamma_5^+$ ) in  $\mathbf{q}$  as  $\langle \Gamma_6^+ | \Gamma_3^+ | \Gamma_6^+ \rangle = \langle \Gamma_6^+ | \Gamma_5^+ | \Gamma_6^+ \rangle = 0$  and the  $\Gamma_4^+$ -component corresponds to the commutator of the components of  $\mathbf{q}$ , which vanishes without a magnetic field. The Hamiltonian is thus

$$\mathcal{H}_6(\mathbf{q}) = E_6 + \frac{\hbar^2 \mathbf{q}^2}{2m_0} A_6 \quad (\text{C1})$$

with the free parameters  $E_6$  and  $A_6$ .

For the  $\Gamma_8^-$ -subspace, the analysis is similar, only that the angular momentum matrices for spin  $I = 3/2$

$$\begin{aligned} I_x &= \frac{1}{2} \begin{pmatrix} 0 & \sqrt{3} & 0 & 0 \\ \sqrt{3} & 0 & 2 & 0 \\ 0 & 2 & 0 & \sqrt{3} \\ 0 & 0 & \sqrt{3} & 0 \end{pmatrix}, \\ I_y &= \frac{i}{2} \begin{pmatrix} 0 & \sqrt{3} & 0 & 0 \\ -\sqrt{3} & 0 & 2 & 0 \\ 0 & -2 & 0 & \sqrt{3} \\ 0 & 0 & -\sqrt{3} & 0 \end{pmatrix}, \\ I_z &= \frac{1}{2} \begin{pmatrix} -3 & 0 & 0 & 0 \\ 0 & -1 & 0 & 0 \\ 0 & 0 & 1 & 0 \\ 0 & 0 & 0 & 3 \end{pmatrix} \end{aligned} \quad (\text{C2})$$

have to be used, and that there are in total 3 parameters for the second-order terms (one for  $\Gamma_1^+$ ,  $\Gamma_3^+$  and  $\Gamma_5^+$  each). This results in the Hamiltonian

$$\begin{aligned} &\mathcal{H}_8(\mathbf{q}) \\ &= E_8 + \frac{\hbar^2}{2m_0} \left\{ A_8 \mathbf{q}^2 + A'_8 \left( \left[ I_x^2 - \frac{1}{3} \mathbf{I}^2 \right] q_x^2 + \text{c.p.} \right) \right. \\ &\quad \left. + A''_8 \{ \{ I_x, I_y \} \{ q_x, q_y \} + \text{c.p.} \} \right\} \end{aligned} \quad (\text{C3})$$

where  $\{I_x, I_y\} = (I_x I_y + I_y I_x)/2$  is the symmetrised product and c.p. denotes the cyclically permuted terms. This is equivalent to the Suzuki–Hensel Hamiltonian in the subspace of the  $\Gamma_8^+$  valence bands.

Dipole transitions between the two conduction bands are allowed at the  $\Gamma$ -point, therefore the lowest-order term in the cross-space is linear in  $\mathbf{q}$  ( $\hat{=}\Gamma_4^-$ ). There is one free parameter, and this part of the Hamiltonian can be constructed from the three matrices that transform as

$\Gamma_4^-$  in the  $\Gamma_8^- \otimes \Gamma_6^+$  cross-space<sup>42</sup>

$$\begin{aligned} U_x &= i\sqrt{\frac{1}{2}} \begin{pmatrix} -1 & 0 \\ 0 & -\sqrt{\frac{1}{3}} \\ \sqrt{\frac{1}{3}} & 0 \\ 0 & 1 \end{pmatrix}, \quad U_y = \sqrt{\frac{1}{2}} \begin{pmatrix} 1 & 0 \\ 0 & \sqrt{\frac{1}{3}} \\ \sqrt{\frac{1}{3}} & 0 \\ 0 & 1 \end{pmatrix}, \\ U_z &= -i\sqrt{\frac{2}{3}} \begin{pmatrix} 0 & 0 \\ 1 & 0 \\ 0 & 1 \\ 0 & 0 \end{pmatrix}. \end{aligned} \quad (\text{C4})$$

The off-diagonal Hamiltonian can then be expressed via

$$\mathcal{H}_{6,8}(\mathbf{q}) = \frac{\hbar}{m_0} B_{6,8} \mathbf{R} \cdot \mathbf{q} \quad (\text{C5})$$

where

$$R_{x_i} = \begin{pmatrix} 0 & U_{x_i}^\dagger \\ U_{x_i} & 0 \end{pmatrix} \in \mathbb{C}^{6 \times 6} \quad (\text{C6})$$

and the complete Hamiltonian is simply

$$\mathcal{H}(\mathbf{q}) = \mathcal{H}_6(\mathbf{q}) + \mathcal{H}_8(\mathbf{q}) + \mathcal{H}_{6,8}(\mathbf{q}). \quad (\text{C7})$$

The parameter of interest for the transitions between yellow and blue series is thus  $B_{6,8}$ .

#### Appendix D: Evaluation of the integrals

The two types of overlap integrals in Eqs. (22) and (23) have been evaluated by using the plane-wave expansion

$$e^{i\mathbf{q} \cdot \mathbf{r}} = 4\pi \sum_{\ell=0}^{\infty} \sum_{m=-\ell}^{\ell} (-1)^m i^\ell j_\ell(qr) Y_\ell^m(\mathbf{n}_\mathbf{q}) Y_\ell^{-m}(\mathbf{n}_\mathbf{r}) \quad (\text{D1})$$

where  $j_\ell(r)$  denotes the spherical Bessel functions. Inserting this into Eq. (23) and integrating over the angular degrees of freedom yields

$$\begin{aligned} W(\tau, \tau', \mathbf{q}) &= 4\pi \sum_{\lambda=|\ell-\ell'|}^{\ell+\ell'} (-1)^{m'} i^\lambda Y_\lambda^{m'-m}(\mathbf{n}_\mathbf{q}) \\ &\times G(\lambda, m-m'; \ell, -m; \ell', m') \int_0^\infty dr r^2 j_\lambda(qr) f_\tau^\dagger(r) f_{\tau'}(r) \end{aligned} \quad (\text{D2})$$

where  $f_\tau(r)$  is the radial part of  $\phi_\tau(\mathbf{r})$  and  $G(\ell_1, m_1; \ell_2, m_2; \ell_3, m_3)$  denotes the Gaunt coefficients

$$\begin{aligned} & G(\ell_1, m_1; \ell_2, m_2; \ell_3, m_3) \\ &= \oint d^2\mathbf{n} Y_{\ell_1}^{m_1}(\mathbf{n}) Y_{\ell_2}^{m_2}(\mathbf{n}) Y_{\ell_3}^{m_3}(\mathbf{n}) \\ &= \sqrt{\frac{(2\ell_1+1)(2\ell_2+1)(2\ell_3+1)}{4\pi}} \\ &\times \begin{Bmatrix} \ell_1 & \ell_2 & \ell_3 \\ 0 & 0 & 0 \end{Bmatrix} \begin{Bmatrix} \ell_1 & \ell_2 & \ell_3 \\ m_1 & m_2 & m_3 \end{Bmatrix}. \end{aligned}$$

The symbols in the curly brackets are the Wigner 3-j symbols. The Gaunt coefficients vanish if  $m_1+m_2+m_3 \neq 0$  or  $\ell_1+\ell_2+\ell_3$  is an odd number.

The other integrals can be evaluated through

$$\begin{aligned} \mathcal{O}(\tau, \tau', \mathbf{q}) &= -4\pi \sum_{\mu=-1}^1 (-1)^{m'-\mu} \langle \ell' + 1, m' - \mu; 1, \mu | \ell', m' \rangle \sum_{\lambda=|\ell'+1-\ell|}^{\ell'+1+\ell} G(\ell, -m; \ell' + 1, m' - \mu; \lambda, m - m' + \mu) i^\lambda \\ &\quad \times Y_\lambda^{m'-\mu-m}(\mathbf{n}_q) \boldsymbol{\xi}_\mu \left[ \frac{\ell' + 1}{2\ell' + 1} \right]^{1/2} \int_0^\infty dr r^2 j_\lambda(qr) f_\tau^\dagger(r) \left( \frac{\partial}{\partial r} - \frac{\ell'}{r} \right) f_{\tau'}(r) \\ &+ 4\pi \sum_{\mu=-1}^1 (-1)^{m'-\mu} \langle \ell' - 1, m' - \mu; 1, \mu | \ell', m' \rangle \sum_{\lambda=|\ell'-1-\ell|}^{\ell'-1+\ell} G(\ell, -m; \ell' - 1, m' - \mu; \lambda, m + \mu - m') i^\lambda \\ &\quad \times Y_\lambda^{m'-\mu-m}(\mathbf{n}_q) \boldsymbol{\xi}_\mu \left[ \frac{\ell'}{2\ell' + 1} \right]^{1/2} \int_0^\infty dr r^2 j_\lambda(qr) f_\tau^\dagger(r) \left( \frac{\partial}{\partial r} + \frac{\ell' + 1}{r} \right) f_{\tau'}(r) \end{aligned} \quad (\text{D3})$$

where  $\langle \ell_1, m_1; \ell_2, m_2 | \ell_3, m_3 \rangle$  denotes the Clebsch-Gordan coefficients, and  $\boldsymbol{\xi}_{-1} = (1, -i, 0)^T / \sqrt{2}$ ,  $\boldsymbol{\xi}_0 = (0, 0, 1)^T$

and  $\boldsymbol{\xi}_1 = (-1, -i, 0)^T / \sqrt{2}$  are the spherical basis vectors.

\* sjard.krueger@uni-rostock.de

<sup>1</sup> J. Frenkel, Phys. Rev. **37**, 17 (1931).

<sup>2</sup> G. H. Wannier, Phys. Rev. **52**, 191 (1937).

<sup>3</sup> E. F. Gross, Il Nuovo Cimento (1955-1965) **3**, 672 (1956).

<sup>4</sup> T. Kazimierczuk, D. Fröhlich, S. Scheel, H. Stolz, and M. Bayer, Nature **514**, 343 (2014).

<sup>5</sup> J. Thewes, J. Heckötter, T. Kazimierczuk, M. Aßmann, D. Fröhlich, M. Bayer, M. A. Semina, and M. M. Glazov, Phys. Rev. Lett. **115**, 027402 (2015).

<sup>6</sup> F. Schöne, S. O. Krüger, P. Grünwald, H. Stolz, S. Scheel, M. Aßmann, J. Heckötter, J. Thewes, D. Fröhlich, and M. Bayer, Phys. Rev. B **93**, 075203 (2016).

<sup>7</sup> F. Schöne, S. O. Krüger, P. Grünwald, M. Aßmann, J. Heckötter, J. Thewes, H. Stolz, D. Fröhlich, M. Bayer, and S. Scheel, J. Phys. B: At. Mol. Opt. Phys. **49**, 134003 (2016).

<sup>8</sup> V. Walther, S. O. Krüger, S. Scheel, and T. Pohl, Phys. Rev. B **98**, 165201 (2018).

<sup>9</sup> J. Heckötter, M. Freitag, D. Fröhlich, M. Aßmann, M. Bayer, P. Grünwald, F. Schöne, D. Semkat, H. Stolz, and S. Scheel, Phys. Rev. Lett. **121**, 097401 (2018).

<sup>10</sup> F. Schweiner, J. Main, M. Feldmaier, G. Wunner, and C. Uihlein, Phys. Rev. B **93**, 195203 (2016).

<sup>11</sup> H. Stolz, F. Schöne, and D. Semkat, New J. Phys. **20**, 023019 (2018).

<sup>12</sup> F. Schweiner, J. Main, G. Wunner, M. Freitag, J. Heckötter, C. Uihlein, M. Aßmann, D. Fröhlich, and M. Bayer, Phys. Rev. B **95**, 035202 (2017).

<sup>13</sup> M. Kurz, P. Grünwald, and S. Scheel, Phys. Rev. B **95**, 245205 (2017).

<sup>14</sup> M. Aßmann, J. Thewes, D. Fröhlich, and M. Bayer, Nature Materials **15**, 741 (2016).

<sup>15</sup> F. Schweiner, J. Main, and G. Wunner, Phys. Rev. Lett. **118**, 046401 (2017).

<sup>16</sup> S. Nikitine, Philosophical Magazine **4**, 1 (1959).

<sup>17</sup> E. Gross, Soviet Physics Uspekhi **5**, 195 (1962).

<sup>18</sup> J. Schmutzler, D. Fröhlich, and M. Bayer, Phys. Rev. B **87**, 245202 (2013).

<sup>19</sup> M. Jörger, E. Tsitsishvili, T. Fleck, and C. Klingshirn, phys. stat. sol. (b) **238**, 470 (2003).

<sup>20</sup> D. Ziemkiewicz and S. Zielińska-Raczyńska, Opt. Lett. **43**, 3742 (2018).

- <sup>21</sup> D. Ziemkiewicz and S. Zielińska-Raczyńska, *Opt. Exp.* **27**, 16983 (2019).
- <sup>22</sup> M. Takahata and N. Naka, *Phys. Rev. B* **98**, 195205 (2018).
- <sup>23</sup> M. Takahata, K. Tanaka, and N. Naka, *Phys. Rev. Lett.* **121**, 173604 (2018).
- <sup>24</sup> P. Grünwald, M. Aßmann, J. Heckötter, D. Fröhlich, M. Bayer, H. Stolz, and S. Scheel, *Phys. Rev. Lett.* **117**, 133003 (2016).
- <sup>25</sup> M. Khazali, K. Heshami, and C. Simon, *J. Phys. B: At. Mol. Opt. Phys.* **50**, 215301 (2017).
- <sup>26</sup> V. Walther, R. Johne, and T. Pohl, *Nature Communications* **9**, 1309 (2018).
- <sup>27</sup> A. Werner and H. D. Hochheimer, *Phys. Rev. B* **25**, 5929 (1982).
- <sup>28</sup> C. Carabatos, A. Diffiné, and M. Sieskind, *Journal de Physique* **29**, 529 (1968).
- <sup>29</sup> G. M. Kavoulakis, Y.-C. Chang, and G. Baym, *Phys. Rev. B* **55**, 7593 (1997).
- <sup>30</sup> T. Itoh and S.-i. Narita, *J. Phys. Soc. Jpn.* **39**, 140 (1975).
- <sup>31</sup> R. G. Waters, F. H. Pollak, R. H. Bruce, and H. Z. Cummins, *Phys. Rev. B* **21**, 1665 (1980).
- <sup>32</sup> K. Suzuki and J. C. Hensel, *Phys. Rev. B* **9**, 4184 (1974).
- <sup>33</sup> M. French, R. Schwartz, H. Stolz, and R. Redmer, *J. Phys.: Condens. Matter* **21**, 015502 (2008).
- <sup>34</sup> J. W. Hodby, T. E. Jenkins, C. Schwab, H. Tamura, and D. Trivich, *J. Phys. C: Solid State Phys.* **9**, 1429 (1976).
- <sup>35</sup> F. Schweiner, J. Main, G. Wunner, and C. Uihlein, *Phys. Rev. B* **95**, 195201 (2017).
- <sup>36</sup> A. Alvermann and H. Fehske, *J. Phys. B: At. Mol. Opt. Phys.* **51**, 044001 (2018).
- <sup>37</sup> A. M. Konzelmann, S. O. Krüger, and H. Giessen, *Interaction of OAM light with Rydberg excitons: Modifying dipole selection rules*, arXiv:1905.07131 (2019).
- <sup>38</sup> C. T. Schmiegelow, J. Schulz, H. Kaufmann, T. Ruster, U. G. Poschinger, and F. Schmidt-Kaler, *Nature Communications* **7**, 12998 (2016).
- <sup>39</sup> A. Afanasev, C. E. Carlson, C. T. Schmiegelow, J. Schulz, F. Schmidt-Kaler, and M. Solyanik, *New J. Phys.* **20**, 023032 (2018).
- <sup>40</sup> L. C. L. Y. Voon and M. Willatzen, *The  $k \cdot p$  Method* (Springer Verlag, Berlin, Heidelberg, 2009).
- <sup>41</sup> J. Luttinger, *Phys. Rev.* **102**, 1030 (1956).
- <sup>42</sup> G. F. Koster, J. O. Dimmock, R. G. Wheeler, and H. Statz, *Properties of the 32-point groups* (1963).
- <sup>43</sup> F. C. Von der Lage and H. A. Bethe, *Phys. Rev.* **71**, 612 (1947).